# Maize domestication phenotypes reveal strigolactone networks coordinating grain size evolution with kernel-bearing cupule architecture

Jiahn-Chou Guan ,<sup>1,2,3,\*</sup> Changsheng Li ,<sup>4</sup> Sherry Flint-Garcia ,<sup>5</sup> Masaharu Suzuki ,<sup>1,2,3</sup> Shan Wu ,<sup>1</sup> Jonathan W. Saunders ,<sup>1</sup> Lemeng Dong ,<sup>4</sup> Harro J. Bouwmeester ,<sup>4</sup> Donald R. McCarty ,<sup>1,2,3</sup> and Karen E. Koch ,<sup>1,2,3</sup>

- 1 Horticultural Sciences Department, University of Florida, Gainesville, Florida 32610, USA
- 2 Plant Molecular and Cellular Biology Program, University of Florida, Gainesville, Florida 32610, USA
- 3 Genetics Institute, University of Florida, Gainesville, Florida 32610, USA
- 4 Swammerdam Institute for Life Sciences, University of Amsterdam, Amsterdam 100 BE, The Netherlands
- 5 United States Department of Agriculture Agricultural Research Service, Columbia, Missouri 65211, USA

J.-C.G. designed the research with input from D.R.M. and K.E.K. If not otherwise stated, J.-C.G. performed the experiments and data analyses. S.W. generated the RNA-seq libraries. J.W.S. helped corn growth in field and greenhouse. C.L., L.D., and H.J.B. measured strigolactone levels. S.F.-G. contributed the teosinte introgression lines. J.-C.G. and K.E.K. wrote the article with significant contribution from D.R.M., M.S., S.F.-G., C.L., and H.J.B. The authors responsible for distribution of materials integral to the findings presented in this article in accordance with the policy described in the Instructions for Authors (https://academic.oup.com/plcell/pages/General-Instructions) is: Jiahn-Chou Guan (guanjc@ufl.edu).

### **Abstract**

Research Article

The maize (*Zea mays*) ear represents one of the most striking domestication phenotypes in any crop species, with the cob conferring an exceptional yield advantage over the ancestral form of teosinte. Remodeling of the grain-bearing surface required profound developmental changes. However, the underlying mechanisms remain unclear and can only be partly attributed to the known domestication gene *Teosinte glume architecture 1* (*Tga1*). Here we show that a more complete conversion involves strigolactones (SLs), and that these are prominent players not only in the *Tga1* phenotype but also other domestication features of the ear and kernel. Genetic combinations of a teosinte *tga1* allele with three SL-related mutants progressively enhanced ancestral morphologies. The SL mutants, in addition to modulating the *tga1* phenotype, also reshaped kernel-bearing pedicels and cupules in a teosinte-like manner. Genetic and molecular evidence are consistent with SL regulation of TGA1, including direct interaction of TGA1 with components of the SL-signaling system shown here to mediate TGA1 availability by sequestration. Roles of the SL network extend to enhancing maize seed size and, importantly, coordinating increased kernel growth with remodeling of protective maternal tissues. Collectively, our data show that SLs have central roles in releasing kernels from restrictive maternal encasement and coordinating other factors that increase kernel size, physical support, and their exposure on the grain-bearing surface.

### Introduction

Remarkable transitions produced the ear of modern maize (*Zea mays* spp. *mays* L.), from the tiny seed head of its wildgrass ancestor, teosinte (*Zea mays* spp. *parviglumis*) (Beadle, 1979). Not only were seed size and number under selection but also the structures that bear them. The pivotal formation

of a cob gave the grain-bearing surface of maize an unsurpassed strength, area, and yield-enhancing architecture. Central to this grain-bearing surface was the restructuring of tissues that previously enveloped each kernel with a hard fruitcase (Figure 1A). The radical retraction of these fruitcases into stems accompanied the extreme compaction of kernel-bearing internodes, adding strength to thickness of

<sup>\*</sup>Author for correspondence: guanjc@ufl.edu (J.-C.G.)

### IN A NUTSHELL

**Background**: The prehistoric ancestor of modern maize (*Zea mays*) is unrecognizable, lacks a cob, and protects each of its tiny kernels inside an acorn-like shell. Evolution of the maize ear during domestication transformed these hard coverings to cob tissue, which not only freed kernels to become the largest known grains but also helped convert spindly stems to the most massive, seed-bearing surfaces of any cereal crop. Only a small fraction of this pivotal conversion is currently understood. We knew from our previous work on overall plant architecture that strigolactone hormones (SLs) could be involved.

**Question**: Could SLs be among the missing factors in evolution of the maize ear from its wild ancestor, teosinte? We hypothesized that SLs could restructure kernel-bearing surfaces of cobs, increase seed size, and coordinate these changes. We also proposed that SLs could regulate a known domestication gene as well as act alone.

**Findings**: A rare combination of domestication features emerged in maize mutants unable to form or sense SLs. Kernels were small, cobs primitive, and seed-bearing cupules larger. Also, when SL-deficient mutants were combined with an ancestral form of the known domestication gene, *Teosinte glume architecture 1 (Tga1*), ears and kernels showed the most primitive, teosinte-like features yet observed. In addition, without SLs coordinating development, rigid seed-bearing cupules often ruptured growing kernels. Finally, analysis of underlying mechanisms indicated that SLs could act alone as well as regulate *Tga1* by sequestering its protein. Evidence included RNA-seq expression analysis, protein–protein interactions, and additional maize genetics.

**Next steps**: We now will intensify our focus on identifying genetic modifiers and other means of modulating SL activity in maize. The results presented here show that impacts could coordinate ear and kernel features in addition to known roles of SLs in maize architecture, mycorrhizal symbioses, and vulnerability to devastation by witchweed (*Striga*) in Africa.

the evolving cob. Withdrawal of these casings also allowed a 10-fold increase in grain mass from teosinte to current-day maize (Flint-Garcia, et al., 2009; Figure 1A). The casing-to-cob transition involved two key structures: the cupule (rachid, stem internode tissue) and the outer glume (persistent floral structure). The cupule (rachid) of teosinte changed from a broad, vertical pocket that enveloped most of the grain, to a much shorter, horizontal, tightly folded structure imbedded in the maize cob (ear axis) (Beadle, 1979). Likewise, the outer glume of teosinte moved from its protective position forming one side of the casing to a small vestigial structure on the cob surface (Figure 1A). The resulting exposure of kernel surfaces and their re-orientation on the ear has facilitated grain expansion as well as harvest and human consumption (Beadle, 1979; Matsuoka et al., 2002; Doebley, 2004; Flint-Garcia, et al., 2009; Piperno et al. 2009).

Thus far, the only identified contributor to this morphological conversion has been *Teosinte glume architecture 1* (*Tga1*), a locus supported by analysis of quantitative trait loci (QTL) and molecular genetic data (Dorweiler et al., 1993; Dorweiler and Doebley, 1997; Doebley, 2004; Wang et al., 2005, 2015; Preston et al., 2012). A partial transition of ear architecture is mediated by the maize *Tga1*, which is a dominant, gain-of-function mutation that arose from its recessive *tga1* progenitor in teosinte (Dorweiler et al., 1993; Dorweiler and Doebley, 1997). The TGA1 protein belongs to the SPL (Squamosa-promoter binding Protein-Like) family of transcription factors that have a wide spectrum of roles in vegetative and reproductive development (Moreno et al., 1997; Chuck et al., 2007, 2010, 2014; Jiao et al., 2010; Miura

et al., 2010; Preston et al., 2012; Wang et al., 2012; Zhu et al., 2013). Despite the importance of this gene in maize domestication, *Tga1* can account for only a fraction of the observed differences between ears of teosinte and modern maize.

Possible roles for strigolactones (SLs) in domestication of the maize ear remain unexplored. The SLs can affect diverse developmental processes in other species, and the vegetative architecture of maize (Guan et al., 2012). These carotenoidderived phytohormones are synthesized primarily in roots and either secreted or transferred upwards through the xylem to above-ground tissues (Al-Babili and Bouwmeester, 2015). The first phytohormone activity recognized for SLs was the control of lateral shoot branching (Gomez-Roldan et al., 2008; Umehara et al., 2008). SL functions are now known to include a breadth of developmental and physiological processes (Al-Babili and Bouwmeester, 2015; Aliche et al., 2020; Chesterfield et al., 2020). Among these roles are contributions to recruitment of beneficial microbes, increased stress tolerance, and modification of agronomic traits, all of which raise prospects for SL applications in agriculture (Aliche et al., 2020; Chesterfield et al., 2020). Rice (Oryza sativa) architecture, especially tillering, is associated with natural variation in SL biosynthesis (Jamil et al., 2012; Cardoso et al., 2014; Sang et al., 2014; Song et al., 2017; Wang et al., 2020), but broader implications of SLs in agronomic traits have received little attention. Initial studies with some crop species have suggested that SL deficiency could lead to decreases in size or biomass of seeds and other reproductive structures (Kohlen et al., 2012; Liu et al., 2013;

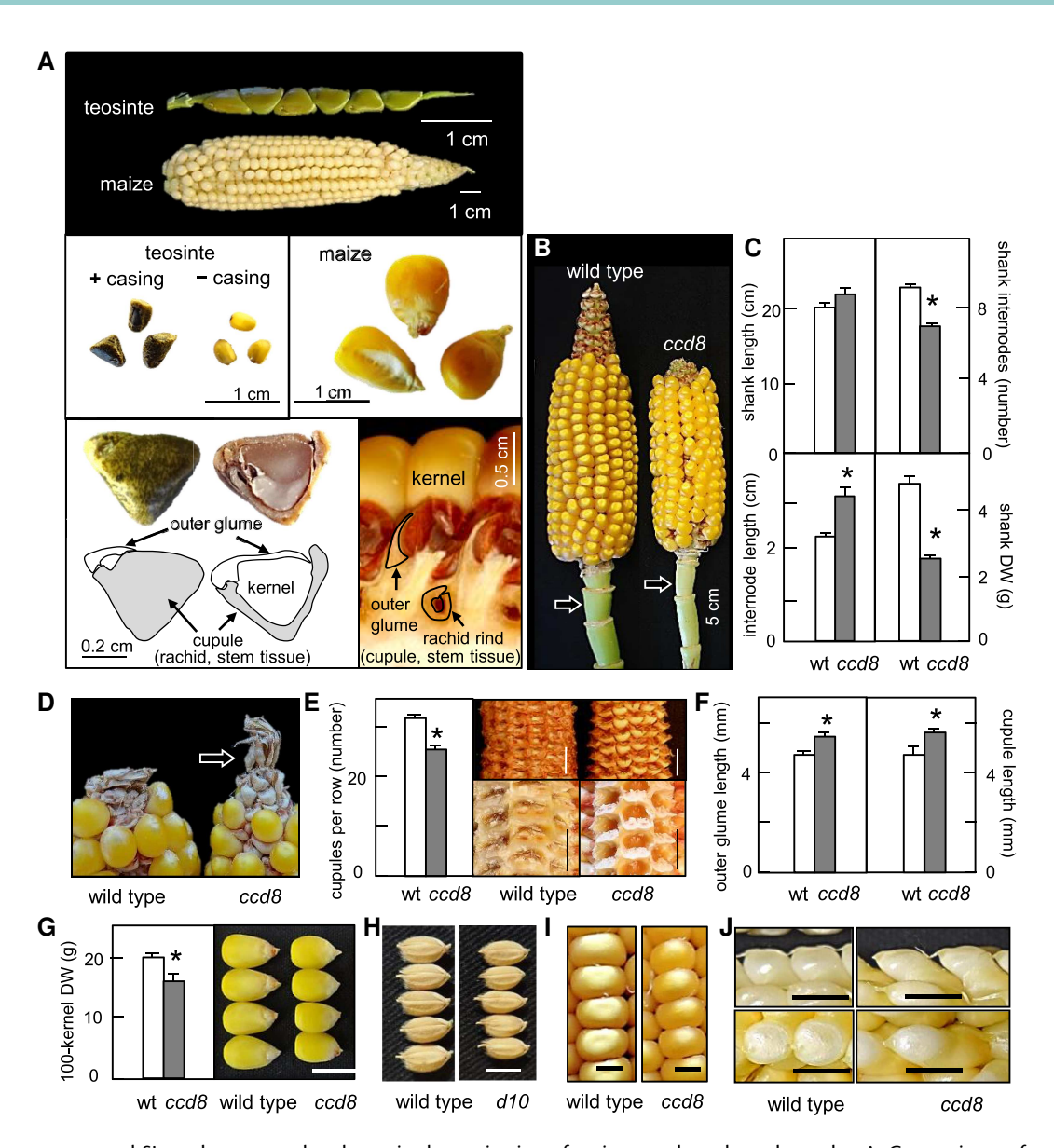


Figure 1 Phenotypes reveal SLs to be among the players in domestication of maize ears, kernels, and cupules. A, Comparisons of ear and kernel morphologies for maize and its ancestor, teosinte. Note the 3.5-fold difference in magnification of teosinte and maize ears imaged at 12 and 10 DAP, respectively (upper panel). Teosinte kernels are approximately 10-fold smaller (middle panel) and each is enveloped by unusual extensions of maternal-stem and floral tissue that form hard, protective fruitcases around them (lower panel). Diagrams and fresh-tissue images show how the fruitcase-to-cob conversion reconfigured two key structures, the cupule (rachid, a stem internode) and the outer glume (a persistent floral structure). B, Impact of SLs on kernel-bearing support structures of ears and shanks from wild-type maize (W22 inbred control) and SL-deficient mutant, ccd8. Arrows indicate single internodes. C, Quantified effects of ccd8 on total shank length, internode number, internode length, and dry weight [means  $\pm$  SEM (standard error of the mean), n = 25]. D, Staminate spikelets (arrow) of an ancestral phenotype (Doebley, 2004) observed at the distal tip of almost half the SL-deficient ccd8 ears (11 out of 24 ears from the spring field of 2010). E, Number of cupules per kernel row (means  $\pm$  SEM, n =24; far right) and diagnostic domestication features of the ccd8 cupule that phenocopy those of the teosinte allele for Tga1 (Wang et al., 2005; left panel). F, Outer-glume lengths from comparable sites on ears (positioned fourth to sixth from the base; means  $\pm$  SEM, n = 48) and average cupule (rachid) lengths (five rows per ear, six ears per genotype, means  $\pm$  SEM, n = 6) determined after removing glumes and kernels from fresh, mature ears, and dividing length of each row by the number of internodes (kernel cupules) as per Dorweiler and Doebley (1997). G, The 100-kernel dry weight of ccd8 and wild-type maize grains (means  $\pm$  SEM, n = 8; left panel) and images of kernel morphology (right; bar = 1 cm). H, Rice-grain phenotypes conferred by mutation of the ccd8 ortholog (d10; bar = 0.5 cm). I, Crowns of mature ccd8 and wild-type maize kernels at 35 DAP (bar = 0.5 cm). J, Morphology and angle of exposure for mid-ear kernels at 8 DAP on ccd8 and wild-type ears (bar = 0.5 cm). (\* indicates  $P \le 0.01$ , t test.)

Pasare et al., 2013; Yamada et al., 2019). Likewise, our previous work in maize showed that ears of an SL-deficient mutant (carotenoid cleavage dioxygenase 8, ccd8) were shorter and

narrower (Guan et al., 2012), a finding indicative of SL impact on the developing female inflorescence and its productivity. Studies from chemical profiling of root exudates and biochemical analysis of biosynthetic enzymes indicate that maize produces a unique mixture of SLs (Yoneyama et al., 2015, 2018, 2020; Charnikhova et al., 2017; Xie et al., 2017). Among them, zealactone (methyl zealactonoate) is the predominant stimulant for seed germination of the devastating root-parasitic witchweeds, *Striga hermonthica* and *Striga asiatica* (Charnikhova et al., 2017; Xie et al., 2017). Recently, the discovery of SL catabolism by carboxylesterases has opened new avenues of manipulation for hormonal roles of SLs and thus their impacts on agriculturally important traits in crops (Roesler et al., 2021; Xu et al., 2021).

Here, we reveal unexpected roles for SLs in maize domestication phenotypes that operate not only through SL regulation of traits previously ascribed to TGA1 alone but also via coordination of other SL-responsive features under selection. We first demonstrated the SL-specificity of distinctive domestication phenotypes in ears and kernels of mutants deficient in SL biosynthesis or signaling. Next, we analyzed genetic combinations of the recessive teosinte tga1 and the SL-deficient maize mutant, ccd8, which uncovered increasingly primitive ear morphologies. We then defined a molecular basis for regulatory input by SLs into action of TGA1 using a combination of yeast two-hybrid (Y2H) and in planta assays for binding by TGA1 to both the SL receptor and specific components of the SL signaling network. We further confirmed these interactions using SL-signaling mutants in maize. A mechanism is thus in place for SL modulation of TGA1. Since this system operates by sequestering target proteins, we additionally demonstrated its potential for enhanced influence when concentrations of TGA1 and its Neighbor Of Tga1 (NOT1) paralog were limiting, a condition caused by the domestication mutation in maize that converts Tga1 to a repressor (Wang et al., 2015). Lastly, we identified distinctive, TGA1-independent contributions by SLs to seed size, pedicel structure, and in-rolling of rachid tissues. We propose a two-step scenario in which domestication of maize would have required an essential, permissive mutation in tga1 that concurrently enhanced its SL-responsiveness while releasing kernels from protective maternal tissues. This conversion would have allowed subsequent selection for additional SL-regulated kernel enlargement (beyond that mediated by TGA1 and NOT1) and further enhancement of specific, yield-related aspects of cob architecture in the female inflorescence. Throughout this process, the

Table 1 Analysis of grain weight from rice SL-pathway mutants and wild-type plants

Genotype	100 grain weight (g)	Reduction percentage (%)
Shiokari	2.74 ± 0.01	•
d17-1	$2.05 \pm 0.01^*$	25.18
d10-1	$2.04 \pm 0.03^*$	25.55
d27-1	$2.26 \pm 0.02*$	17.52
d14-1	$2.11 \pm 0.04$ *	22.99

<sup>\*</sup>P < 0.001 (ANOVA). Values are means  $\pm$  SEM (n = 3). Shiokari is the wild-type background of rice dwarf (d) mutants.

SL signaling network would have been poised to coordinate developmental changes in maternal and kernel tissues.

### Results

### SL-specific domestication phenotypes in the ear of *ccd8* maize

Our first goal was to determine the extent to which SLs regulate the structure of modern-maize ears and kernels. To this end, we focused on distinctive domestication-related aspects of SL-deficient ccd8 maize. We showed previously that this pleiotropic phenotype included a smaller ear (Guan et al., 2012; Figure 1B) in addition to the excessive vegetative branching shared with SL-deficient mutants in other species and with the ancestral teosinte (Guan et al., 2012). We thus looked closely at SL roles in ear size and related domestication features of ccd8. The SL-deficiency does not lead to longer ear shanks (lateral branches; Figure 1, B and C); however, fewer shank internodes in ccd8 were countered by greater elongation of each (about 40% more). Shank dry weight also dropped markedly in the mutant (about 50% less), which was noteworthy given the role of this structure in physical support and nutrient supply to the ear (Figure 1C). In addition, SL-deficiency enhanced the portion of ccd8 ears forming stamens at their distal tips (a primitive feature; Doebley, 2004) to almost half (46%, 11 out of 24 ears) compared to 8% (2 out of 25 ears) in wild-type controls (Figure 1D). Importantly, a closer examination of ccd8 ears after kernel removal revealed key changes in cupule number per row (20% less than wild type) and their structure (Figure 1E). In particular, the glumes and cupules that form a protective cover around the teosinte kernel were enlarged in maize ears if SLs were lacking (Figure 1F). Outer glumes and cupules were both about 20% longer in the mutant. This distinctive phenotype, especially the modified glumes and cupules, has thus far been seen only in association with the known domestication gene, Tga1 (Dorweiler et al., 1993; Dorweiler and Doebley, 1997; Wang et al., 2005). In addition, the size and dry weight of ccd8 kernels decreased by around 22% relative to wild-type controls (Figure 1G). To determine whether this role of SLs in seed size is also conserved in rice (Oryza sativa L.), we quantified grain weights for three SL-deficient rice mutants, dwarf10 (d10), dwarf17 (d17), and dwarf27 (d27), and one SL-signaling mutant, dwarf14 (d14), that encode CCD8, CCD7, an isomerase, and an SL receptor, respectively. Seed weights of all mutants were reduced by 17%-25% (Figure 1H and Table 1). Results are consistent with analysis of these rice mutants by Yamada et al. (2019). The maize and rice data together implicate a broad relevance for SL signaling in mediating seed size during grain development of crops. In addition, grain shape was affected, with the SL-deficient ccd8 kernels having more rounded domes at maturity compared to the flatter, wild-type tops (Figure 11). During early development, the mutant maize kernels were also narrower, more pointed, and grew at an angle closer to the axis of ear elongation (Figure 1J). These results indicate central roles for SL signaling in the transition from primitive ear and kernel structures to modern-day ears and exposed kernels.

Three strategies were used to test the hypothesis that the ear and kernel-size phenotypes observed here were due solely to the SL deficiency caused by the ccd8 mutation. The first approach was to identify a ccd8-specific revertant that restored normal function to an otherwise isogenic mutant. This process required a reversal of the same insertion event that created the ccd8::Ds mutant allele by disrupting the wild-type sequence with a Dissociation (Ds) element. To initiate this excision, we generated homozygous, Ac-active, ccd8 plants by introducing an immobilized Activator (Ac::im; Vollbrecht et al., 2010) into the ccd8-mutant line. Two generations of self-pollination produced enough material for a seedling-stage screen using the yellow-stripe leaf feature of the ccd8 phenotype as a convenient visual marker for revertants. We thus identified a green-leafed revertant after evaluating about 1,200 ccd8 maize seedlings (F3; Figure 2A). The revertant status was confirmed by two diagnostic changes in the CCD8 gene sequence. First, the Ds insertion was absent. Second, an important, imperfect repair during the Ds excision created a readily distinguishable, single-nucleotide C-to-G transversion. This change converted an arginine (R) to a glycine (G) at position 426 of the CCD8 protein (Figure 2, B and C). Comparative analysis of this site indicated that the Ac/Ds reversion had created a distinctive, new allele not evident in any maize inbreds or teosinte lines (Figure 2B). To determine whether this revertant allele encoded a functional enzyme, a complementation test was performed by overexpressing the new CCD8<sup>R426G</sup> allele in an Arabidopsis thaliana ccd8 mutant (max4-6; Guan et al., 2012). As predicted, the CCD8<sup>R426G</sup> allele successfully rescued the SL-deficient phenotype of Arabidopsis max4-6 plants, bringing their otherwise short stature and abundant branching to wild-type levels (Col-0; Figure 2D). The rosette branch numbers for 15 out of 29 independent transgenic lines were far below those of max4-6 mutants at 3 weeks after flowering (Supplemental Table 1). The CCD8<sup>R426G</sup> revertant allele thus encoded a functional enzyme for SL biosynthesis. In addition, at all stages of maize development, the phenotype of revertant maize plants was indistinguishable from that of inbred (wild type) controls with functional, unaltered CCD8 genes (Figure 3A). Importantly, the phenotypic equivalency was clearly apparent for ear morphology, kernel size, and overall rachid length (Figure 3A). The revertant allele described here provided an especially effective genetic confirmation that the ear and kernel-size phenotype of ccd8 resulted specifically from impaired SL biosynthesis.

The second approach to test whether the rachid phenotype of *ccd8* arose specifically from SL deficiency was to apply steady-state levels of the synthetic SL analog, *rac-*GR24, to the *ccd8* mutant (Figure 3B). To do so, we devised a stringfeeding method for delivery of either GR24 or a control solvent (DMSO). By threading cotton strings through the stem

with a sewing needle, a wicking system was established in which the two ends of each string could absorb and transfer fluid from small, tightly wrapped vials of solution (typically 2-mL microcentrifuge tubes; Figure 3B). Uptake into each plant was quantified as the depletion of liquid volume in the sets of sealed vials. Treatments were applied to both mutant and wild-type plants. The GR24 supplements decreased rachid length of *ccd8* mutants to that of wild-type plants (Figure 3B). In contrast, DMSO controls showed no effect. These results further support the direct and specific role of SLs in the structure of the kernel-bearing cupule and the rachid in particular, both of which are characteristic of modern maize.

The third approach was to test whether specific disruptions to SL signaling could duplicate the cupule and kernel phenotypes observed in ccd8 mutants. The key to this strategy was perturbation of the SL receptor (D14) encoded in maize by two homologous genes, D14a (Zm00001d028294) and D14b (Zm00001d048146). To develop the required mutants, we characterized Mu-insertion alleles from the UniformMu (McCarty et al., 2013) and Mu-Illumina (Williams-Carrier et al., 2010) populations (4 alleles for D14a and 3 alleles for D14b; Supplemental Figure 1). Possible hybrid effects were avoided by five generations of back-crossing Mu-Illumina materials into the W22 inbred (UniformMu genetic background). As expected, no visible phenotypes were evident in any of the single mutants due to the extensive sequence similarity between D14a and D14b proteins (95%) and their predicted functional redundancy. In contrast, double mutants of d14a-4 and d14b-3 (Supplemental Figure 1) showed plant and ear morphology comparable to ccd8 mutants (Figure 3C). Shared phenotypes included additional lateral branches (two more) and shorter ears (reduced by 43%). In particular, cupules of double mutants (d14a/d14b) had rachid rinds that were similarly widened, elongated, and invaginated as those of ccd8 ears. Collectively, this evidence further supports a role of SL signaling in maize ear architecture and seed development.

# Ear phenotypes regulated by SL-deficient ccd8 and alleles of the domestication gene Tga1

Commonalities in underlying mechanisms for SLs and the domestication gene *Tga1* were implicated by the distinctive phenotypic features they shared and by their previous attribution to TGA1. To test the extent of overlap at the genetic level, we developed a *ccd8/tga1* double-recessive line (*tga1* being a non-mutant recessive ancestor). The *tga1* parent line was created by introgressing the teosinte *Tga1* allele (*tga1*) into the W22 inbred (Dorweiler et al., 1993; Wang et al., 2005). We initially hypothesized that a fully shared path would be evident for SL and *tga1* given the known role of TGA1 in glume and cupule phenotypes. If so, the double-recessive ears would resemble those of *tga1* single recessives. Unexpectedly, additional and even complementary effects of the *ccd8* and *tga1* genes were evident (Figure 4A).

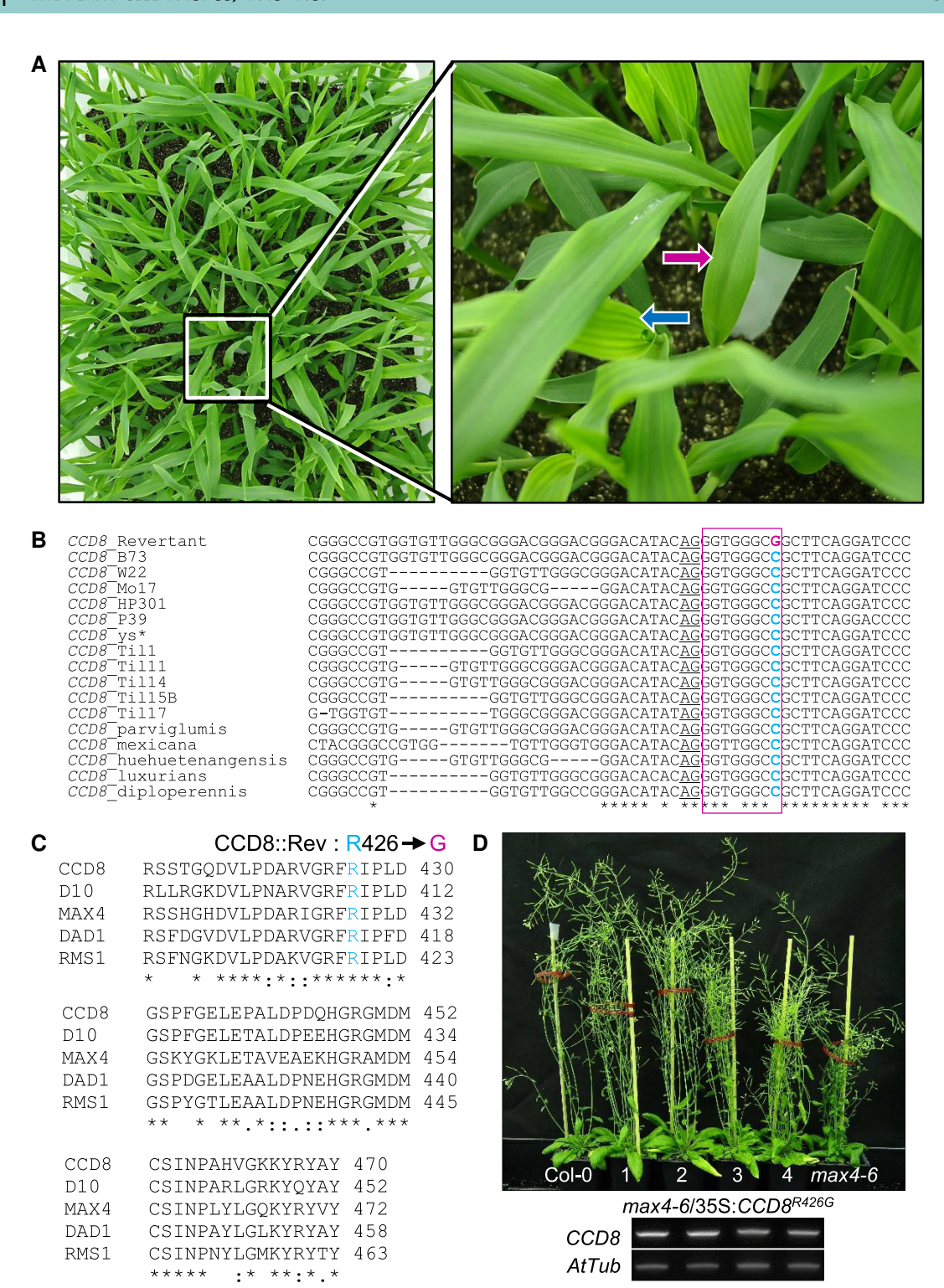


**Figure 2** A revertant *CCD8* allele was identified and characterized. A, High-throughput screening for a naturally occurring revertant of the *ccd8* mutant. Fourteen day-old *Ac*-active *ccd8* seedlings grown in a plastic bin were screened for leaves without the yellow-stripe phenotype. The juvenile leaf of a revertant (magenta arrow heading to the right) did not show the yellow-stripe leaf phenotype typical of *ccd8* mutants (blue arrow heading to the left). B, Nucleotide sequence alignment of the revertant *CCD8* allele (*CCD8::Rev*) with other *CCD8* alleles from diverse maize inbreds and teosintes. Only the regions flanking the *Ds* insertion site are shown. The red box indicates the 8-bp direct repeat induced by the transposon insertion. The revertant allele has a C-to-G transversion (red letter), which is at the 3'-end of the direct repeat. This transversion changes the codon of "CGC" for arginine (R) to "GGC" for glycine (G). There is no polymorphism detected at the place of the conserved nucleotide "C" (blue) in maize inbreds or teosintes. The underlined "AG" is the left border of the second intron. C, Partial amino-acid alignment of CCD8 orthologs from rice (D10), Arabidopsis (MAX4), petunia (DAD1), and pea (RMS1). Alignment is shown where encoded by the *Ds* insertion-flanking region. The arginine

Although the length of double-recessive ears was intermediate between that of the singles (ccd8 and tga1), their diameter was significantly smaller (by 11% and 20%, respectively; Figure 4A). Of special interest in double recessives was the prominent size of cupules. In teosinte, cupules envelope the grains, whereas they form unusually large, cradle-like cavities under developing kernels in the double recessive (Figure 4A). Cupules of double recessives were about 30% longer than those of single recessives (Figure 4A). At the same time, cupule width was greater for only the tga1 recessives, while those of ccd8 mutants were significantly narrower, opposite effects that left the width of tga1/ccd8 cupules unchanged (Figure 4A). The importance of these morphologies is their progressive enhancement of an ancestral phenotype with more vertical cupules and decreasing width-to-length ratios. These dimensions dropped from 1.9 in wild type (inbred control) to 1.5, 1.4, and 1.2 in tga1, ccd8, and double-recessive cupules, respectively. A full spectrum of this gradation in verticality is depicted in Figure 4B together with that initially observed by G. W. Beadle for modern maize to teosinte, including ancient ear morphology (Beadle, 1979; Ramos-Madrigal et al., 2016). Cupules of tga1/ccd8 shown here closely resemble those of maize x teosinte hybrids. When young ears of these genotypes are compared to those of teosinte (Figure 4C), rachid rinds of cupules can be seen extending outward around the kernel like a pair of protective arms that hold both the kernel and outer glume close to the stem axis. This configuration is especially prominent in teosinte but was also recapitulated in the double recessive tga1/ccd8, indicating that this ancestral state can be restored particularly well by the combination of a recessive tga1 and SL deficiency. However, the long axis of each glume was aligned with that of the ear such that these protective structures restricted perpendicular growth of kernels. Co-ordination was thus lost between expansion of enveloping maternal glumes and that of developing kernels. Consequently, the hard, protective glumes often damaged expanding kernels by distorting, rupturing, and even decapitating them (Figure 4D). Collective distortion of doublerecessive kernel shape by both glumes and cupules is evident in Figure 4D, along with the more pointed tips of these grains. In addition to their altered shape, the size of double-recessive kernels was also reduced by 23% and 38% relative to ccd8 and tga1 single recessives, respectively (Figure 4E). Collectively, these data support a contribution of SL signaling to the enhancement of kernel accessibility on the ear surface by aiding coordination of kernel enlargement with reduction of cupule and glume development during ear formation. We also tested the hypothesis that SLs mediate cell-level features of the outer glumes and rachid rinds in their conversion to structures as occurred during domestication (Dorweiler and Doebley, 1997). In modern maize, the outer glume is essentially vestigial, whereas its ancestral form provided a hard, lignified covering for the outer face of the kernel. Here, a partial restoration of the ancestral outer-glume morphology was evident in both the single recessive (ccd8) and tga1) and the double-recessive genotypes (Figure 4). However, a cell-level investigation revealed important differences, including evidence consistent with distinct, but overlapping roles for SLs (ccd8) and tga1. Both recessives increased cell length and cell number, but to differing degrees depending on position in the organ. In modern maize, cells of the outer, abaxial mesophyll are only slightly elongated (Dorweiler and Doebley, 1997), and to a lesser extent in the distal half of the glume (Figure 5A). This is consistent with the straightening of glumes and their reduced intrusion into the kernel-development space. In contrast, cells in this outer, abaxial layer of ccd8 are smaller throughout the glume, and their greater number is responsible for the increase in overall length of this organ. Cell numbers also increased in the tga1 glume, but as observed in previous work (Dorweiler and Doebley, 1997), this enhances both thickness and length of the structure. In addition, cells between the abaxial and adaxial layers of parenchyma in tga1 glumes are elongated with spirally lignified cell walls (Figure 5). Double-recessive glumes showed features of both ccd8 and tga1. Although cell number did not increase to the degree observed for tga1, the small cell size, thick cell walls, and dense packing led to a particularly hard glume with a pronounced curl into the kernel-development (Figure 5A, tga1/ccd8). Results indicate that both SLs and TGA1 regulate induration of maize glumes through their impact on shape and size of abaxial cells.

Architecture of the cupule cavity showed still more prominent roles for SLs and their proposed interaction with TGA1. Both the teosinte *tga1* allele and the SL-deficient *ccd8* mutation were required for the most effective recapitulation of a teosinte-like cupule (Figure 5B). A key change centered on the rachid rind, a layer of hypodermis lining the innermost cavity of the cupule. This structure is tightly curled (360°) and deeply imbedded in the cob of modern maize. However, the rachid rind uncurled slightly in the presence of teosinte *tga1* (322° arc) and strongly uncurled in the SL-deficient *ccd8* genotypes (184° and 148° arcs in *ccd8* and

#### **Figure 2** (Continued)

(R) residue(blue) is conserved in all species and was replaced by a glycine (G) in the revertant CCD8 (CCD8::Rev). D, The newly identified, second allele of the CCD8<sup>R426G</sup> shows a potentially valuable, partial complementation of the excessive-branching typical in *ccd8* mutants such as the Arabidopsis *max4*–6. Note that the height of transgenic plants is greater than that of mutant (*max4*–6) and comparable to wild type (Col-0). The revertant allele is driven by a constitutive expression promoter (CaMV35S) and its relative expression was quantified by RT-PCR. Data for each transgenic plant is shown in an ethyl bromide-staining agarose gel (bottom panel). Expression of the Arabidopsis *Tubulin* (*AtTub*) gene provides an internal expression control.

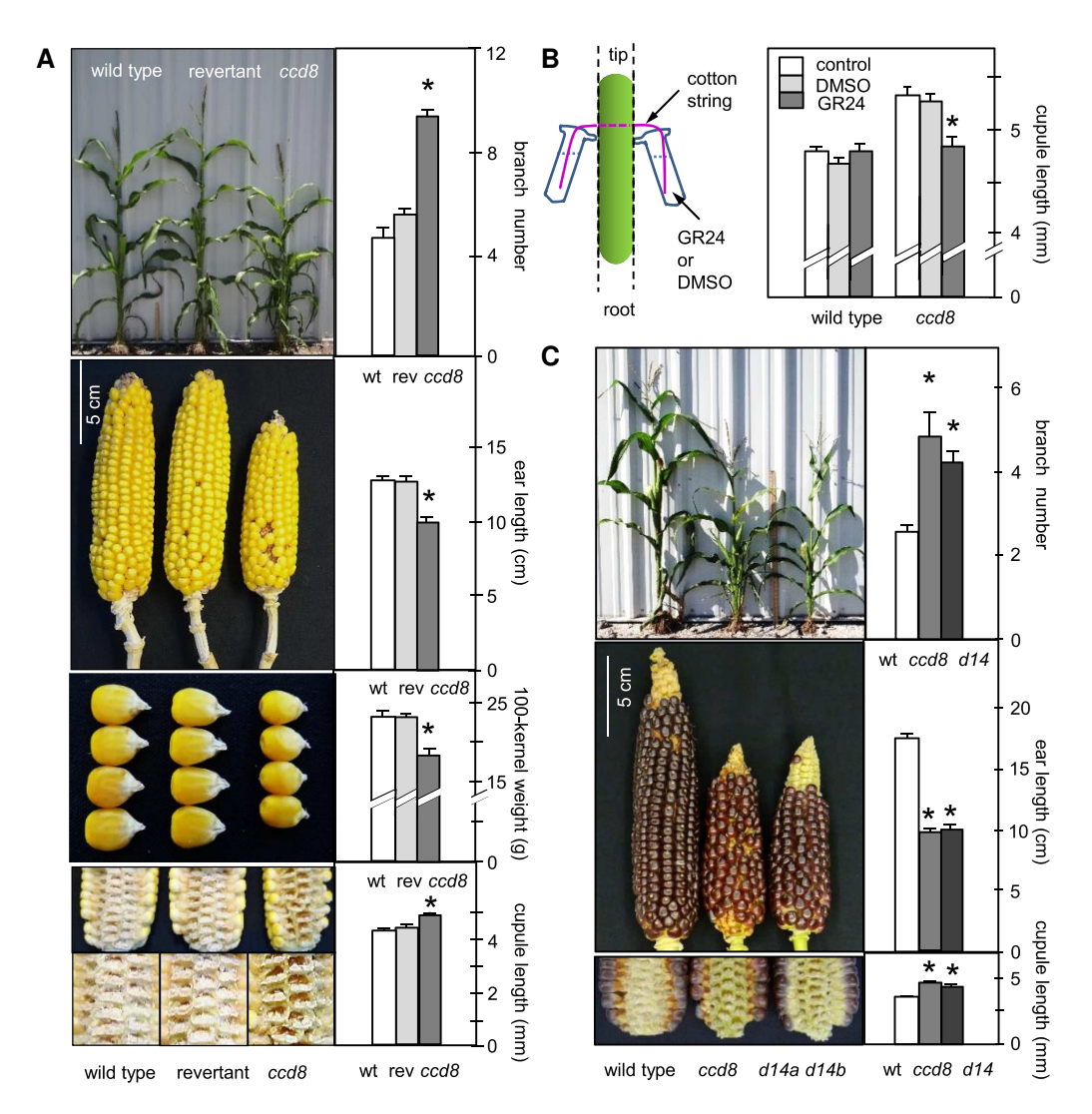
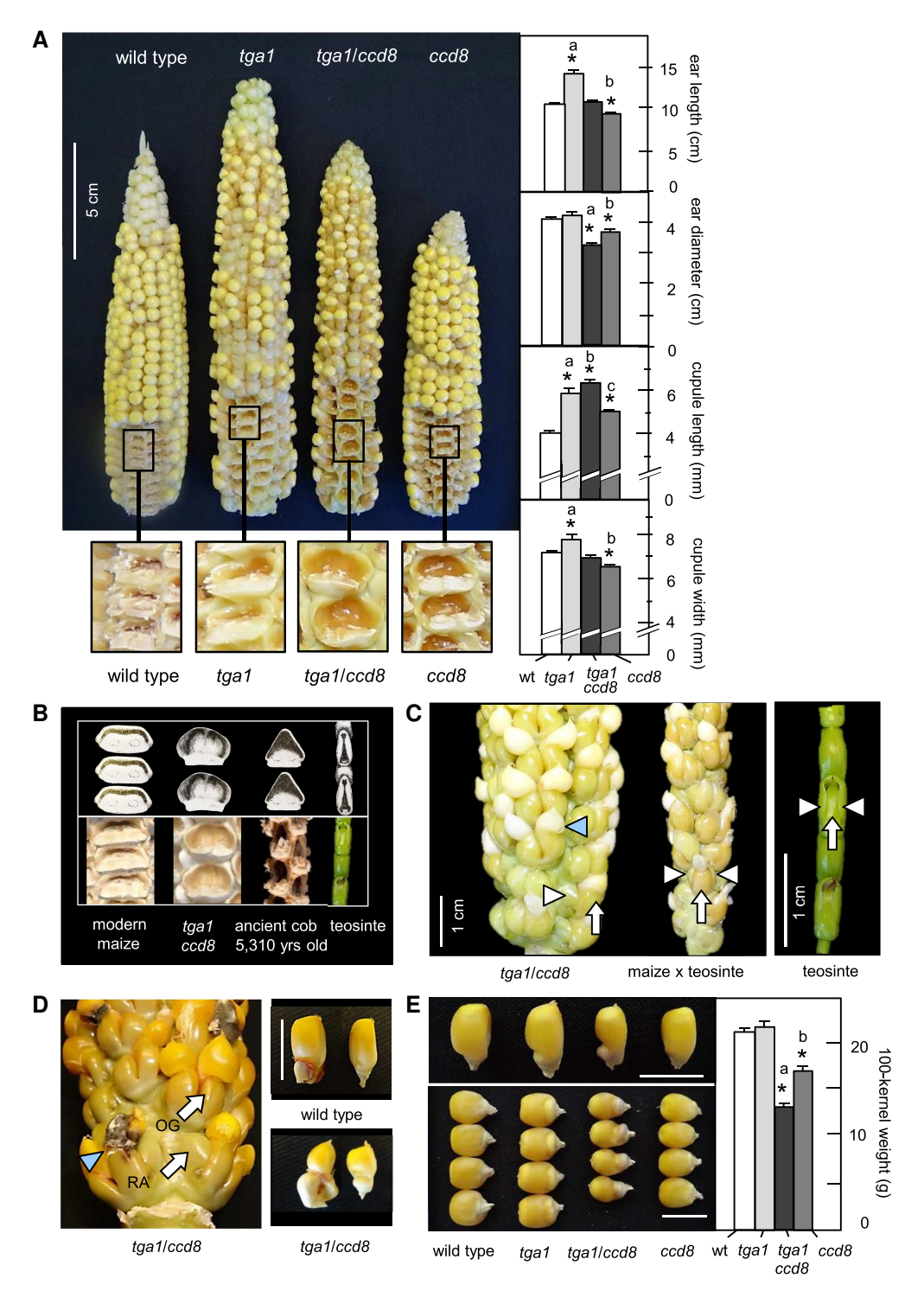


Figure 3 Three lines of evidence support SL-specificity of the *ccd8* domestication phenotype. A, A confirmation-by-reversion rescue of the *ccd8*-mutant phenotype by excision of its causal transposable element. Comparisons of wild-type, revertant, and *ccd8*-mutant phenotypes for plant architecture (top), ear and shank morphology (second panel), kernel size and shape (third panel), and cupule structure (bottom; means  $\pm$  SEM, n = 14, n = 10, n = 6, and n = 4, respectively; \* indicates differences between revertant and *ccd8* mutant at  $P \le 0.01$ , t test). B, Pharmacological complementation of the SL-deficient *ccd8*-mutant phenotype using a string-wick delivery (left) to supply a synthetic SL analog (*rac-*GR24 at 1  $\mu$ M) or DMSO (0.02% trace solvent control) and compare to additional controls without wicking strings. Quantified responses of cupule lengths (right; means  $\pm$  SEM, n = 6, \* indicates difference between GR24 and either of the controls at  $P \le 0.01$ , t test). C, Phenocopy of the SL-deficient, *ccd8* mutant by disruption of the SL-signaling system at its SL receptor (D14) evident in structural images (left) and quantifications (right) for plant form and branch number (top), ear shape and length (middle), and rachid structure and length (bottom; means  $\pm$  SEM, n = 14, 10, and 18, respectively, \* indicates difference at  $P \le 0.01$ , t test). (See Supplemental Figure 1 for generation of the dysfunctional *d14* maize line [double for *d14a/d14b*].) Note that the genetic background for this set of comparisons is the color converter W22 inbred.

tga1/ccd8, respectively). When SL was lacking, the rachid rind uncurled and extended into a flatter shape like that of teosinte (193° arc). Strictly comparable sections were centered through glumes and pedicels. Effects of tga1 and ccd8 predominated in different tissues, with tga1 primarily impacting glumes and ccd8 primarily affecting cupules. The influence of tga1 on overall cupule size was mediated largely by its effect on thickness of the glume and pedicel (Figure 5B). Nonetheless, synergistic effects of SL deficiency and teosinte tga1 were apparent at the cell level in the cupule, where reduced thickness and extended length were observed in both

single and double recessives (Figure 5B and Table 2). In double recessives, a greater portion of the cupule was comprised small, highly lignified cells (Figure 5B). These results indicate a prominent contribution of SLs to the cupule changes underlying modern ear architecture, and further, that both SLs and TGA1 do this by modulating cell shape, size, and cell wall structure. Alterations in pedicel shape were also mediated by both TGA1 and SL, with deficiency of the latter leading to a near right-angle bend in the pedicel that moves its upper, kernel-bearing region into a position essentially parallel to the long axis of the ear (as in teosinte). When the

(continued)



**Figure 4** Distinctive ancestral ear and kernel features are mediated by independent and overlapping contributions from SL deficiency and the Tga1 teosinte allele. A, Ear and cupule morphologies of wild type (W22 inbred control), teosinte tga1 (introgressed into W22), SL-deficient ccd8, and tga1/ccd8 double recessive (teosinte tga1 being a nonmutant, recessive ancestor). Ears were imaged at 14 DAP (about 1/2 mature; left) with exposed cupules enlarged below and morphological quantifications at right. (means  $\pm$  SEM, n=10 for ears, n=6 ears for cupules, \* indicates difference between wild type and mutants at  $P \le 0.01$ , t test, lower-case letters show differences between genotypes). B, Progression of cupule shape from horizontal to vertical along a gradient from modern maize (left) to primitive teosinte (right) in diagrams above [cupules other than tga1/ccd8 were redrawn from Beadle (1979)] and photographic images below. The image of a 5,310-year-old cob was adapted from Ramos-Madrigal et al. (2016) with permission from Elsevier (License # 5431490269821). C, Cupule constraints to kernel expansion in young ears of the tga1/ccd8 double recessive (left), a maize  $\times$  teosinte hybrid (center), and teosinte (left), showing outer glumes (white arrows), outer edges of enveloping cupules

teosinte allele of *tga1* is also present, the bent pedicel is markedly thickened (Figure 5B; see also below).

# Molecular dissection of the proposed interface between TGA1 and the SL signaling network

To address molecular-level aspects of the interface between SL signaling and TGA1, we generated and compared RNA-seq. profiles from immature ears (2.5–3.0 cm) of wild type (W22 inbred control), recessive-mutant (ccd8), recessive-ancestral (nonmutant teosinte tga1), and the double-recessive combination (tga1/ccd8) plants. This developmental stage immediately precedes detectable differences in phenotypes of the mutant and nonmutant Tga1 alleles. Since our genetic and structural analyses were consistent with overlapping, as well as independent effects of ccd8 and tga1 on ear features, we expected to see evidence of both in the RNA-seq data. Results indicated extensive commonalities between effects of the SL signaling network and that of TGA1. Over half of the genes that were upregulated two-fold or more in tga1 ears were also upregulated in the absence of SLs (ccd8; 53%; Figure 6A). The same was observed for downregulated genes, indicating that TGA1 and SL signaling share common direct and/or independent paths in their mediation of ear development. Most of these genes have putative roles in transcriptional regulation, cell division, protein metabolism, or cell wall biosynthesis (Supplemental Data Set 1). Among the latter were 15 sequences that encoded putative enzymes for cell wall quality and lignin biosynthesis (Sekhon et al., 2011), consistent with the enhanced lignification of ccd8 and tga1/ccd8 glumes and rachid rinds described here. Further analysis of the putative lignin biosynthetic genes in the maize genome indicated that the most prominent enhancement in expression included that of Phenylalanine ammonia lyase (PAL), Ferulate (coniferyl alcohol/aldehyde) 5-hydroxylase (F5H), p-Coumarate 3-hydroxylase (C3H), Cinnamate 4-hydroxylase (C4H), and 4-Coumaric acid CoA-ligase (4CL; Supplemental Data Set 1). The nature and extent of this shared regulation spurred further investigation into possible points of control, our first target being the interface between SL signaling constituents and TGA1 itself.

To test the physical basis for potential interactions between the SL signaling network and TGA1, we began with three key players of the SL signaling pathway (Bürger and Chory, 2020; Chesterfield et al., 2020). All three of these, D53, D14, and D3, are named for the DWARF vegetative phenotype (Ishikawa et al., 2005) that results from a deficiency in SL signaling. The first of these proteins, D53, operates by sequestering targets like UNBRANCHED2/

UNBRANCHED3/TASSELSHEATH4 (UB2/UB3/TSH4; Liu et al., 2021) through direct or indirect interaction. The D53 protein is a class I Clp ATPase that lacks a DNA-binding domain (BD) of its own, but acts as a negative regulator of SL signaling (Jiang et al., 2013). The way D53 exerts this control is by aiding sequestration of transcription factors into inactive complexes (Bürger and Chory, 2020). The second protein, D14, operates as a dual-function SL receptor and deactivator of SLs. The third, D3, is also known as MAX2 (More AXillary branching 2) in Arabidopsis, where its role as an F-box protein in an SCF (Skp1-Cullin-F-box) E3 ubiquitin ligase complex mediates ubiquitination of D53 for degradation by the 26S proteasome. This breakdown of D53 releases the initially sequestered transcription factor in an SL-dependent manner. The entire process depends on SL-dependent interactions among these three components, which thus control availability of target transcription factors (like TGA1 in this instance).

To investigate the possibility of direct interaction between these SL signaling components and TGA1, we utilized the toxic effects of TGA1 overexpression on cell viability. The toxicity was evident in our initial yeast work and consistent with an inability to recover viable calli when TGA1 was used in vectors by Wang et al. (2015). The extent of this impact enabled tests of protein-protein interactions in planta as well as in Y2H assays. For both approaches, all DNA constructs were expressed using an improved bimolecular fluorescence complementation (BiFC) vector (Gookin and Assmann, 2014) designed for this dual-purpose use. Here, transient expression of TGA1 in leaf tissue of Nicotiana benthamiana induced chlorophyll loss and necrosis in the agro-infiltrated areas (Figure 6B). In contrast, leaves remained normal and green at sites transformed with maize orthologs of either D53 (Zm00001d023208) or D14a (Zm00001d028294; Figure 6B). The deleterious effects of TGA1 persisted when the Tga1 gene was co-expressed with either D53 or D14a, but not when all three genes were transfected together (Tga1, D53 and D14a). The toxic effect of excess TGA1 in leaves was thus mitigated if the two key participants in the SL signaling pathway were also present (Figure 6B). The mitigation did not appear to require additional SLs, since none was applied exogenously to inoculated leaves. Results were quantified by analysis of chlorophyll content in the infiltrated areas (Figure 6C), which also showed that the consistently deleterious effects of TGA1 alone or with either D14a or D53 were countered only when all three genes were co-expressed. To determine whether the toxic effect on leaf discs resulted specifically from TGA1, we deleted the seven-residue core (HNRRRRK, from amino acid (aa) 172 to

### Figure 4 (Continued)

(white triangles), and a site of kernel rupture (blue triangle). Teosinte ears are imaged prepollination, others at 12 DAP. D, Ear and kernel features of the tga1/ccd8 double recessives (left) showing teosinte-like extensions of outer glumes and cupules (white arrows) and sites where these have ruptured kernels (blue triangle). Comparison of wild-type kernels (upper right) and those of tga1/ccd8 double recessives (lower right) at 35 DAP, with and without their outer glumes (left and right, respectively). E, Kernel profiles and abaxial faces (left) and seed weight (right) of all four genotypes (wild type, tga1, tga1/ccd8, and tga1/ccd8

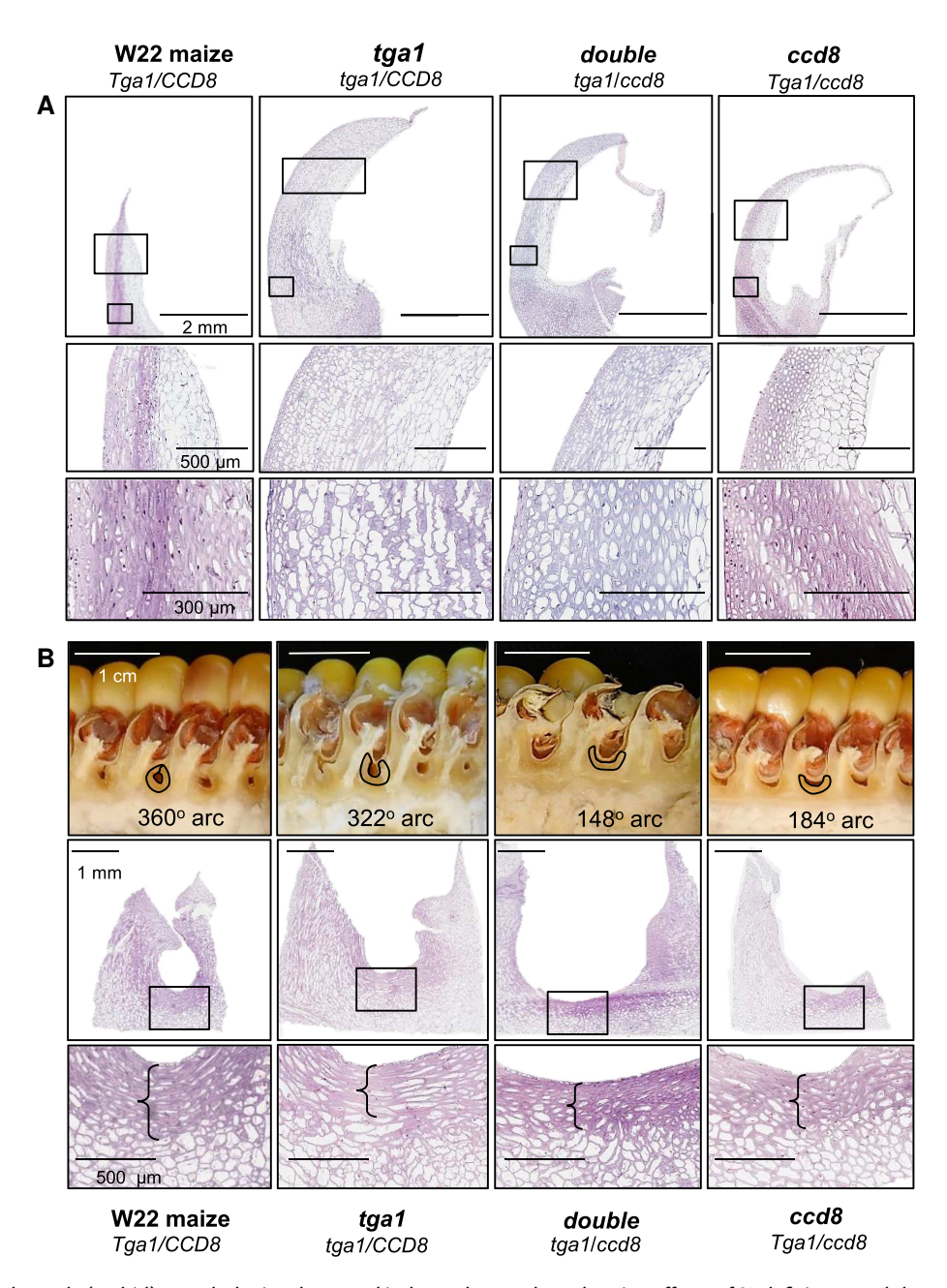


**Figure 5** Glume and cupule (rachid) morphologies also reveal independent and overlapping effects of SL deficiency and the teosinte allele of *Tga1*. A, Sagittal sections through the centers of outer glumes at 10 DAP (about 1/3 mature). Entire outer glumes (top) with boxed areas enlarged below (middle and bottom). B, Sagittal faces of cupules (outlined in black) in fresh, mature ears at 35 DAP (above) and in sections from 10 DAP (middle) enlarged below (bottom). Strictly comparable locales were centered using pedicels and glumes. For fresh-tissue images, one of the two side-by-side kernels in each cupule pocket of modern maize (teosinte has only one) was removed to clarify the profile of maternal tissues. Rachid rinds are visible as elongated hypodermal cells lining the cupule cavity.

Table 2 Depth and cell number in mesoderm layer of rachid rinds

Genotype	Depth of long-cell layer (μm)	Cell number
Wild type	480.03 ± 15.23	$14.7 \pm 0.9$
ccd8	358 ± 9.14**	$12.3 \pm 0.7$
tga1	378.43 ± 19.12*	$12.3 \pm 0.7$
tga1/ccd8	253.53 ± 13.94**	11 ± 1*

<sup>\*</sup>P < 0.05 (ANOVA); \*\*P < 0.01 (ANOVA). Values are means  $\pm$  SEM (n = 3).

178) of the putative nuclear localization sequence in its SBP box and tested the modified construct (TGA1 $^{\Delta7}$ ). No chlorophyll loss or necrosis was observed in leaf discs transfected with the TGA1 $^{\Delta7}$  alone or together with D53, indicating that it was indeed TGA1 that specifically triggered deleterious effects in the infiltrated leaf discs. As shown in Figure 6D, interactions among TGA1, D14a, and D53 were implicated by the strong

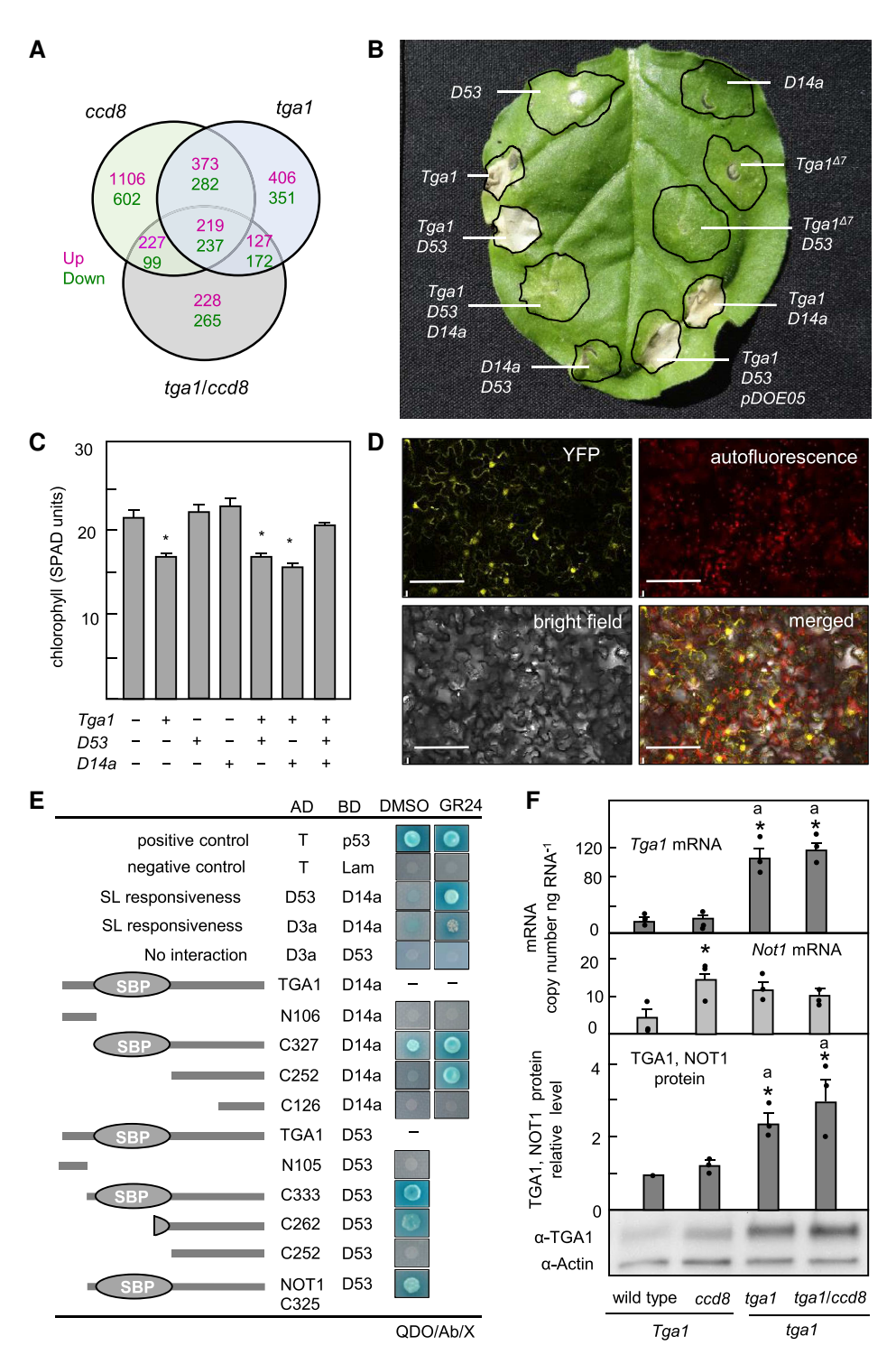


Figure 6 Molecular interactions between the SL-signaling network and that of TGA1 regulate ear and kernel development. A, Venn diagram for DEGs in prepollination ears (2.5–3.0 cm) for each of three genotypes (ccd8, tga1, tga1/ccd8) relative to wild-type controls (W22). Differences greater than two-fold were included for genes upregulated (magenta text at the upper row) or downregulated (green text at the lower row). B, Transient-expression assays in *Nicotiana benthamiana* leaves for in vivo interactions between TGA1 and two key proteins of the SL-signaling system in maize, D53 and D14a. Toxic effects of overexpressing TGA1 (Wang et al., 2015) identify *in planta* interactions with other proteins that modify this response. A single leaf was used for each set of experiments, with TGA1 transfected alone and in combination with one or more proteins of the SL-signaling system as shown (agroinfiltration sites outlined in black, combinations of cultures in white text). C, Chlorophyll content at agroinfiltrated sites in replicate experiments 6 days after infiltration (means  $\pm$  SEM, n = 6, \* indicates difference from control at  $P \le 0.01$ , t test). D, Tobacco leaf mesophyll imaged 48 h after agroinfiltration with BiFC transient-expression constructs carrying maize Tga1 together with D53 (pDOE06-TGA1:

fluorescent signals of complemented monomer Venus fluorescent protein (mVen) in leaf cells where the three genes were concurrently expressed (Figure 6D). To test the specific involvement of TGA1 as the source of fluorescent signals, we fused the small C-terminal fragment of mVen to both D14a and D53, thus limiting fluorescence to instances where TGA1 was present. For contrast, images from combinations of different constructs are shown in Supplemental Figure 2. These results support a physical interaction among TGA1, D14a, and D53 proteins, as well as the specific importance of TGA1.

Strigolactones-shaped ear evolution

We next used Y2H assays to corroborate the in planta tests of protein interactions. We first confirmed that known interactions between SL signaling proteins in other systems (Gomez-Roldan et al., 2008; Umehara et al., 2008) operated similarly in maize. As predicted, the SL receptor (maize D14a) could interact in an SL-dependent manner with the maize F-box protein, D3a (Zm00001d045313), and separately with the transcription co-repressor, D53. Their SL-responsiveness was demonstrated using the SL analog rac-GR24 (Figure 6E). To analyze interactions with TGA1, we circumvented the potential for self-activation observed in fusions to the Gal4 DNA-BD by focusing on assays using TGA1 fusions with the Gal4 activation domain (AD). The full-length TGA1-AD fusion suppressed growth of yeast cells and thus interactions could not be analyzed; nonetheless, AD fusions with separate fragments of TGA1 allowed us to identify regions that interacted in the presence or absence of GR24. The maize D14a interacted directly with the SBP box of TGA1 regardless of whether GR24 was present. However, GR24 enhanced this interaction as well as broadening the interface to include a strongly SL-dependent domain immediately adjacent to the SBP box of TGA1. Similar analysis of D53 binding to strategically truncated TGA1 fragments showed that interaction was limited to a 10-aa domain (from aa 171 to 180) of the SBP box. Further evidence from the TGA1 paralog, NOT1, showed that a comparable region of this protein could interact with D53 (Figure 6E). Conservation of this domain interaction in NOT1 provides additional molecular evidence for an interface with the SL signaling system. Moreover, Wang et al. (2015) showed that Not1 is a direct target of TGA1 repression. Consistent with proposed SL

modulation of this TGA1 activity, we observed a ~two-fold increase in Not1 mRNA levels in SL-deficient genotypes (Figure 6F). We also found upregulation of Tga1 mRNA levels in the recessive tga1 background, an effect not seen by Wang et al. (2015). This divergence is likely attributable to differences in developmental staging. Nevertheless, combined TGA1 and NOT1 protein detected by antibody rose two-fold in the absence of the maize TGA1 (dimerizing repressor; Figure 6F). Results are consistent with the model below for contributions of SL signaling to ear architecture through effects on TGA1 protein function, stability, and/or abundance of NOT1 and TGA1 proteins.

### A model for SL regulation of TGA1

To further evaluate the possible role of SLs in regulating TGA1, we proposed and tested a model based on known mechanisms of SL signaling (Figure 7). We also present this model in the context of contrasting abundance and functionality of TGA1 protein in maize and teosinte. The maize TGA1 is a known repressor that downregulates expression and protein abundance of its closely related Not1 paralog (see data above [Figure 6F] and Wang et al., 2015). This decrease in NOT1 levels would proportionally enhance the impact of SL signaling on sequestration of TGA1 and NOT1 proteins, thus curtailing their action in maize (Figure 7). In contrast, the teosinte TGA1 is not a repressor, so Not1 expression and protein levels rise, allowing the collective NOT1 and TGA1 abundance to overwhelm the SL signaling system (thus minimizing SL-responsiveness). Here we focused on the SL signaling mechanisms in maize, where combined results from our assays above indicated that TGA1 and NOT1 could interact with both D53 and D14, and that this in turn could suppress action of TGA1 as a transcription factor. By analogy with the known function of D53 in SL signaling networks, D53 would bind TGA1 (or NOT1) in a complex (aided here by D14) until the SL-sensing system (including SL responses of both D14 and D3) triggered breakdown of D53 and subsequent release of the TGA1. All interactions involved in this model

### Figure 6 (Continued)

NmVenus/CVenus:D53), and D14a (pDOE05-NmVenus/D14a:CVenus; ×20 magnification, scale bars = 100 μm). E, Interactions between TGA1, D3a, D14a, and D53 in Y2H assays with bait proteins expressed as fusions with Gal4 DNA-BDs and prey proteins with Gal4 ADs. Blue colonies (Y2HGold) indicate protein-protein interactions under high-stringency conditions (see Methods). Specificity of SL-responsive interactions is shown using the synthetic SL analog, rac-GR24 and DMSO controls. A Known affinity between p53 and the large T-antigen (T) provided a positive control for interactions, and a noninteracting lamin (Lam) was used with the T-antigen for a negative control (see Methods). Progressively truncated TGA1 constructs are diagrammed (left) and named (right) to indicate the remaining protein region (N-terminal or C-terminal) and its length in numbers of amino acids. Ovals indicate the SBP (Squamosa-promoter Binding Protein) domain. F, Levels of mRNA for Tga1 and its paralog Not1 (upper panels) together with abundance of encoded protein (lower panel) in developing ears (2.3-2.8 cm) of wild-type controls, ccd8, tga1, and ccd8/tga1. Absolute expression of Tga1 and Not1 mRNAs were determined using corresponding cDNA fragments as standards (\* indicates increased expression of Not1 at  $P \le 0.01$ , t test, with lower-case letters for expression of the teosinte allele of Tga1, means  $\pm$  SEM, n = 3, and dots indicating data from individual bio-replications). The combined abundance of TGA1 and NOT1 proteins is compared between genotypes using anti-TGA1 serum that recognizes both the teosinte and maize TGAs as well as their NOT1 paralog (provided by Dr. John Doebley). Relative levels of the TGA1/NOT1 protein are shown above a representative protein gel blot (\* indicates increases at  $P \le 0.05$ , ANOVA and Tukey-Kramer HSD test, with lower-case letters for differences between relative protein levels, means  $\pm$  SEM, n = 3, and dots indicating data from individual bio-replications).

are supported by molecular evidence from the two in vivo systems shown above and are consistent with conserved components of SL signaling mechanisms in other species. Since D53 acts as a negative regulator by sequestering its targets in complexes, knockouts of D53 should free TGA1, which in maize would suppress glume and cupule development. If so, then d53 mutants would lack elongated glumes and cupules, as well as suppress the ear phenotypes of ccd8 mutants by releasing TGA1 from its complexed form.

To test this prediction of D53 function in maize, we identified two Mu-insertion alleles of d53 from the UniformMu (McCarty et al. 2013) and Mu-Illumina (Williams-Carrier et al., 2010) maize mutant resources and focused on d53-2 due to its coding sequence disruption (Figure 8A). As hypothesized, the modified SL signals resulting from a dysfunctional d53-2 led to responses typical of SL abundance, even in the SL-deficient ccd8/d53 double mutant (Figure 8B). The well-studied inhibition of lateral branching by SL signals was lacking in the ccd8 mutants (Guan et al., 2012), but fully countered in double mutants with d53-2 (Figure 8B). Similar signals of SL abundance also negated effects of SL deficiency in the shortening of ccd8 ears (Figure 8B). Particularly relevant to the model above was the impact of d53-2 on reverting the elongated cupule length of the SL-deficient ccd8 mutant back to the shorter dimensions of domesticated, wild-type maize. Collectively, the genetic evidence presented here supports our hypothesis that the maize SL signaling network enhances key ear domestication traits, and could do so in part by modulating the availability of the maize TGA1 protein.

Our primary aim was not to determine whether CCD8 itself was a domestication gene, but rather to use this SL-deficient mutant to elucidate the role of SLs in domestication phenotypes of the maize ear. We were nonetheless interested in the extent to which CCD8 might have been under selection during domestication or modern breeding. We therefore amplified, sequenced, and compared the CCD8 alleles from six maize inbreds and five teosinte inbreds (Supplemental Figure 3). Data indicated that protein sequence was mostly conserved (Supplemental Figure 3B). Sequences allowed primer design (Supplemental Figure 3C) and allele-specific quantification of CCD8 mRNA levels. The maize CCD8 alleles were more strongly expressed in maize than were the teosinte alleles in teosinte and were at least two-fold to over four-fold greater depending on the maize inbreds and teosinte accessions tested. In addition, expression of teosinte CCD8 alleles rose when introgressed into B73 maize (Liu et al., 2016) where CCD8 mRNAs are normally more abundant but remained two-fold lower than those of endogenous alleles (Figure 9A). Results indicate the presence of a regulatory mechanism in or near the teosinte CCD8 itself. The potential for these differences in CCD8 expression to affect SL profiles of young ears cannot be determined using current technologies (Ravazzolo et al., 2019), but emerging methods allowed quantification of SLs in root exudates of 2-week-old seedlings (Figure 9B). When measured in this

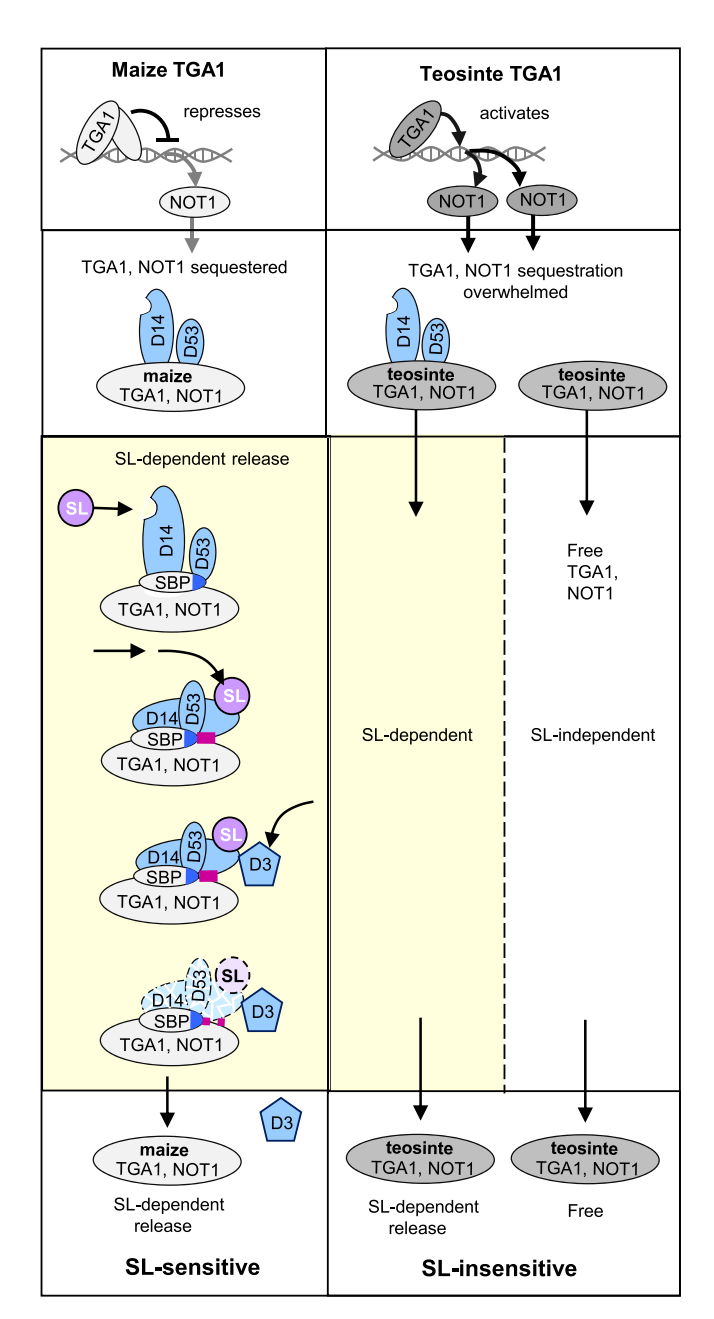


Figure 7 A putative mechanism is diagrammed for SL-responsiveness and its acquisition by maize TGA1. Protein-level impacts of repression by maize TGA1 (light gray ovals) and activation by teosinte TGA1 (dark gray ovals; upper panels), with subsequent abundance affecting sequestration by SL-signaling components (blue ovals; based on data in Figure 6 and Wang et al., 2015). Release of TGA1 and its NOT1 paralog (light yellow panels) begins when SL (lavender circle) binds to its D14 receptor (blue). Conformational changes in D14 expand its TGA1 interaction beyond the SBP box (internal oval) to adjacent sequences (bright pink) and initiate binding between D14 and D53 in the sequestration complex. Subsequent action by D14 recruits the ubiquitination system via D3, which completes the release of TGA1 and NOT1 by targeting the D53 protein for degradation (D14 follows). This progression halts in the absence of SL (as in the ccd8 mutant), leaving sequestered TGA1 to remain complexed with D53 and D14. The two-fold decrease in abundance of TGA1 and NOT1 protein in maize (Figure 5) would

(continued)

way, SL profiles in teosinte exudates varied markedly compared to those of maize, with an especially large range for zealactone, the major SL. Although much lower zealactone levels were detected from many root exudate samples of teosinte relative to maize (Figure 9B), overall no significant difference was evident between maize and teosinte. As with other domestication features, variability may have decreased during selection (Flint-Garcia et al., 2009). In addition, the exudate does not necessarily reflect the production or transport of SLs. The elevated CCD8 expression in developing ears (Guan et al., 2012) implies a potential for localized SL biosynthesis in this major sink organ. Moreover, domestication of teosinte may have selected for partitioning of SLs to above-ground roles as opposed to the possibly greater requirements for SL exudation by roots to aid mycorrhizal associations of teosinte.

The overall elevation of CCD8 expression in maize relative to teosinte suggested a possible target of selection in the regulatory regions of the gene, so we surveyed these zones using the genotypic data (179 single-nucleotide polymorphisms, SNPs) of 1,210 maize lines and the "Diversity" program at MaizeSNPDB (Zhou et al., 2019). Two regulatory regions were identified (about -350 and -800 bp relative to the transcription start site) that showed modest reductions in nucleotide diversity of improved maize lines (Figure 9C). This narrowing in nucleotide diversity is consistent with a possible selective advantage during maize improvement, but its magnitude is minor compared to known domestication genes.

We thus took a broader look at the SL signaling network responsible for key domestication phenotypes to identify other genes in this system that bore signatures of domestication or improvement. Analysis of RNA-seq data from ccd8-mutant ears revealed 44 candidate genes for domestication and 77 for improvement (Hufford et al., 2012), each showing at least a two-fold level of SL-responsive expression (Supplemental Data Set 2). Several prominent candidates of selection included SL-regulated phytohormone genes for lateral organ development and other mRNAs for control of trehalose-6-phosphate (T6P) levels that provide putative signals of sucrose abundance. A drop in levels of this T6P would be favored by respective down- and upregulation of genes for its biosynthesis (T6P synthase, TPS) and metabolism (T6P phosphatase, TPP) that occur when SLs are lacking. Additional SL-regulated candidates of selection include Fructokinase-1 (upregulated), Sugary2/Starch synthase 2 (downregulated), and a transketolase (downregulated).

### Figure 7 (Continued)

allow a greater impact of the SL-signaling system (bottom panels). Each of the SL-signaling components is orthologous to its counterpart in rice, where D53 is a transcription co-repressor, D14 is an SL receptor, and D3 is an F-box protein in the ubiquitin proteasome pathway (Chesterfield et al., 2020). Each interaction shown here is also supported by molecular evidence from two *in vivo* systems (Figure 6) and genetic data here and elsewhere. (For clarity, proteins are not diagrammed in proportion to actual size.)

### Impacts of grain-bearing cupules on kernels within them: Roles of SLs and TGA1

Lastly, Figure 10 places kernel configuration and size together with full silhouettes of the distinctive cupule phenotypes mediated by ccd8 and Tga1. These include fruitcase-to-cob transitions of glumes, cupules, and pedicels, as well as yield-enhancing increases in seed size and accessibility. A primitive teosinte-like glume is characteristic of both recessive alleles studied here (tga1 and the SL-deficient ccd8), but more pronounced for tga1 (Figure 10, top). Most importantly, although both recessives also enlarge the cupule, tga1 does so primarily by thickening the glume and pedicel, whereas ccd8 broadens the cupule cavity by unfolding the pronounced curl at the cupule base (shown in magenta in Figure 10, row 2). Together, tga1 and ccd8 in the double recessive generate the most teosinte-like cupule architecture yet observed. The SLs also have a prominent role in restructuring pedicels such that the portions directly supporting each kernel lie parallel to the ear axis (as in teosinte). The vascular path to kernels is similarly altered (Figure 10, row 3). Seed accessibility is still more prominent, as are seed-size effects, the latter evident in Tga1- and SL-mediated kernel-weight phenotypes (Figure 10, row 4). Impacts of Tga1 on grain size are most apparent when SLs are lacking, and otherwise are potentially masked by additional SL-responsive seed-size factors. The most notable effects of ccd8 are shared with teosinte and include a primitive cupule architecture and small-seed size.

### Discussion

We show here that SLs have a potentially two-fold role in maize domestication and improvement including first, an independent SL contribution to distinctive phenotypes that enhances the grain-bearing surface, pedicel shape, and seed size, and second, SL-regulation of Tga1-mediated alterations in kernel size, ear diameter, and proposed interactions in cupule structure. The magnitude and SL-responsiveness of these domestication traits is demonstrated using diverse molecular approaches together with mutants in SL biosynthesis and signaling (Figures 1-4). Of particular importance are the SL impacts that extend beyond those of TGA1 on seed size (Figures 1 and 4) and newly resolved aspects of the maternal architecture (Figure 5). The latter include SL regulation of teosinte-like pedicels and kernelbearing cupules. An underlying basis for proposed SL control of Tga1 is defined via the molecular and genetic analyses in Figures 6–8. The dramatic relationship between maternal architecture and positioning of kernels is evident in composite morphological analyses of contributions by Tga1 and SLs (as ccd8; Figure 10). Overall, our data are consistent with SLs as major players in the ongoing process of maize domestication regardless of whether individual genes in the SL signaling system were under selection (ccd8 was used here to uncover SL roles). In addition, the present work reveals a breadth of SL-responsiveness among domestication traits that provides a critical mechanism for coordinating progressive restructuring of maternal features with those of seed size increases.

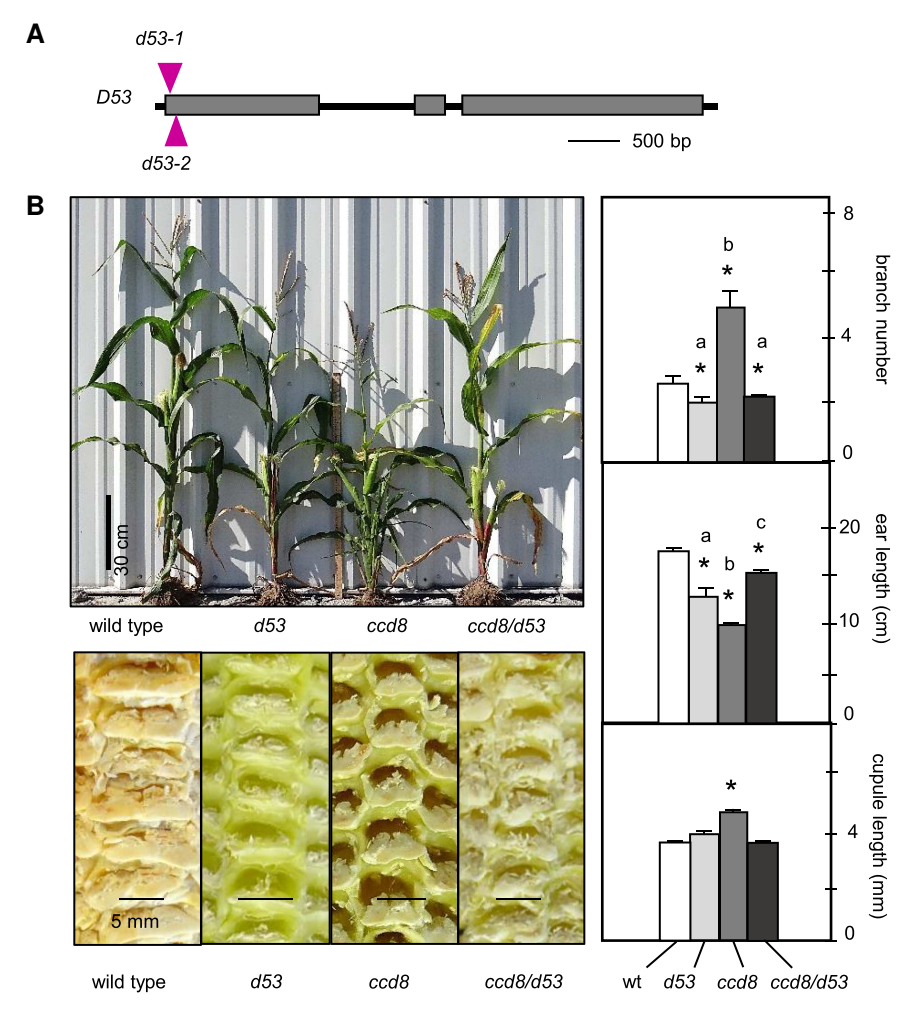


**Figure 8** Suppression of branching, ear length, and cupule phenotypes in *ccd8* mutants by loss of D53 function. A, Diagram of maize *D53* gene structure with coding sequences (gray boxes) and sites of insertion (magenta triangles) for two different *Mutator* transposon insertions (*d53-1* and *d53-2*). B, Whole-plant and branching phenotypes (above) and ear cupules (below) with quantifications of branch number, ear length, and cupule length at the right (means  $\pm$  SEM, n = 14, 10 and 18, respectively, \* indicates differences between wild type and each mutant at  $P \le 0.05$ , with lower-case letters for differences between genotypes by t test and Tukey HSD).

A potentially direct role for SL signaling in domestication is supported by two observations. First, our results show that Tga1 is itself a SL-response factor. Thus, SL signaling is integral to the maize Tga1 phenotypes that were under positive selection during domestication. Second, our results delineate a distinct set of Tga1-independent SL-regulated traits that are of central importance to formation of the modern-maize ear (see summary in Figure 10). Key roles of SLs that are independent of Tga1 include their separate contributions to effects on seed size and especially cupule architecture (a pivotal and minimally understood domestication feature). The SL traits noted here would have been opened to additional selection following the advent of Tga1, since this mutation would have (1) removed physical constraints to SL-mediated kernel expansion, (2) facilitated SL coordination of growth by maternal and filial tissues, and (3) relieved limiting capacity of SL receptors for sequestration caused by overwhelming levels of TGA1 and NOT1 protein. Without these changes, selection on SL signaling may have had less impact. In any case, due to the number of genes involved in SL signaling, domestication signatures distributed over multiple genes may escape detection, and it is likely that additional genes in the complex SL biosynthesis and signaling pathways remain to be discovered.

Genetic data are consistent with impacts of SL signaling that include both independent effects and direct regulation of TGA1. Potential interactions are clearer for kernel size and some aspects of ear morphology but less so for cupule architecture. Additivity in structural features of cupules (Figures 4, 5, and 10) conferred by the tga1/ccd8 combination cannot be interpreted classically as evidence of independent pathways because teosinte tga1 is a wild-type allele rather than a loss-of-function mutation. Although recessive to the Tga1 mutant of maize, teosinte tga1 (1) is expressed, (2) encodes a functional protein, (3) is self-activating, and (4) acts redundantly with the Not1 paralog. The TGA1/NOT1 proteins are

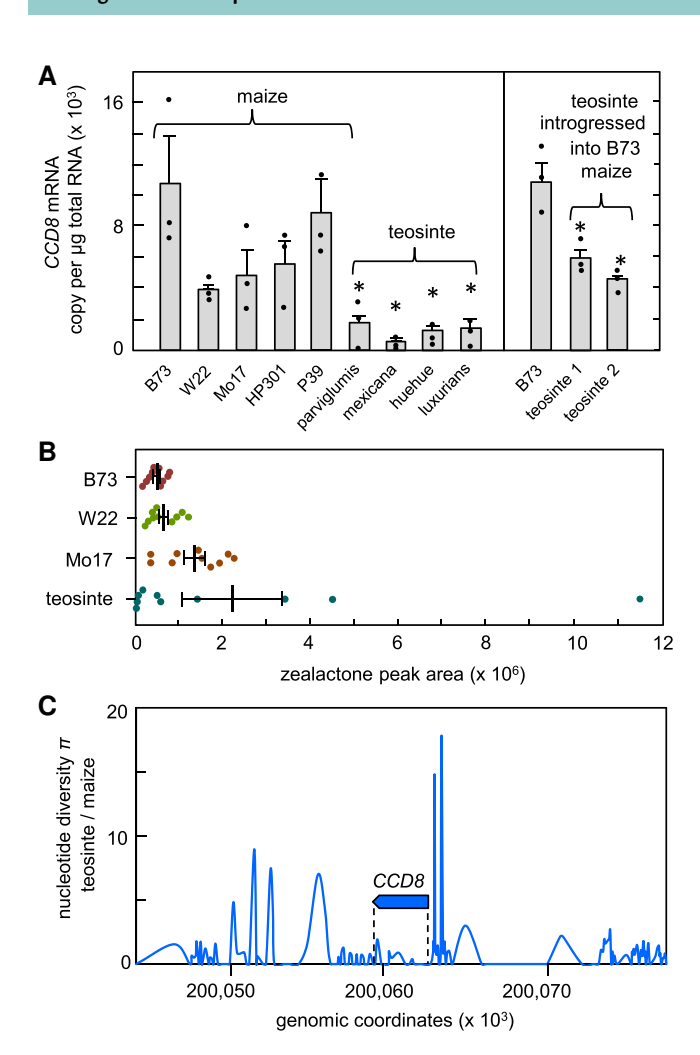


Figure 9 Maize and teosinte differ in their CCD8 expression, SL content, and nucleotide diversity of their CCD8 alleles. A, Abundance of CCD8 mRNAs in maize and teosinte (left panel). Transcript levels of teosinte CCD8 alleles after introgression into maize (right panel). Absolute expression levels of CCD8 were determined using the CCD8 cDNA fragment as a standard. Roots were sampled from 14-day-old seedlings. Maize inbred lines and teosinte subspecies tested appear on the x axis (huehuetanengensis is shortened to "huehue"). Bars show copy number of CCD8 mRNA per microgram of total RNA. Values are means  $\pm$  SEM (n=3). Asterisks indicate a statistically significant difference between the wild-type allele (W22 or B73) and each teosinte allele  $(P \le 0.05, t \text{ test}; \text{dots indicate data from individual bio-replications})$ . B, Quantification of zealactone levels in exudates of maize and teosinte roots. The major form of SL, zealactone, was quantified by LC-MS/ MS in root exudates from seedlings of maize inbreds (B73, W22, and Mo17) and teosinte after 2 weeks of culture in 50-mL falcon tubes. Zealactone levels were determined by calculating area under the peak at m/z 377 > 97. C, Comparison between nucleotide diversity of maize and teosinte lines in the genomic regions flanking their CCD8 gene. Divergence in the genomic region is indicated by the teosinte/ maize ratio for nucleotide diversity from the two populations. The x axis indicates coordinates of the genomic region surrounding CCD8.

thus both present in maize and teosinte to interact with SLs in a manner consistent with our molecular data and model. We would not expect a strictly epistatic interaction even if

SLs acted solely through TGA1/NOT1. A related consideration is that the teosinte *tga1* allele by itself confers only a small portion of the teosinte phenotype. Substantial input from additional genes is thus implicated yet other than a complex QTL on chromosome 3L (Doebley, 2004), the expected modifiers have eluded discovery. We suggest that SL-related genes may be one class of such modifier.

A prominent aspect of this work is its delineation of regulatory mechanisms that could allow the SL signaling network to modulate input by TGA1 into yield-related components of the kernel-bearing surface and of seed size itself. Dissection of the interface between SL signaling and the TGA1 network revealed prominent commonalities in modes of action. At the transcript level, overlap extended to half the genes differentially expressed in ears of the recessive tga1 and a third of those in the SL-deficient ccd8 (Figure 6A). Analysis of individual mRNAs upregulated in all three genotypes (ccd8, teosinte tga1, and tga1/ccd8) showed that SL-modulated genes in the TGA1 network included those for lignin biosynthesis with potential roles in rigidity of outer glumes. In addition, SL deficiency altered expression of genes for production and consumption of T6P, a putative signal of sucrose abundance, that would reduce levels of this signal (mRNAs for TPS and TPP were respectively down- and upregulated in the absence of SLs). Data also indicate genes for secondary contributions by other phytohormones such as observed by Dong et al. (2019) for TB1 control of a different, core domestication network that modulates vegetative architecture. Interactions with auxin could be particularly important given the potential for SL impact on PIN-based auxin transport (Zhang et al., 2020) and for sugar-mediated repression of auxin-enhanced SL signaling (Bertheloot et al., 2020). Collectively, our results are consistent with a SL network that includes interactions with other plant growth regulators as well as sugar substrates and signals (Doll et al., 2017; Koch and Ma, 2017).

Further resolution of network structure and interactions emerged from identifying two points of direct molecularlevel interface between the SL signaling system and the TGA1 regulatory network. Focus was targeted to maize orthologs of proteins with conserved functions in SL signaling, since these would have potentially analogous roles in maize and a predicted capacity for interaction with TGA1. The combination of in planta and Y2H assays (Figure 6) confirmed the potential for TGA1 to be sequestered through interaction with D53 and D14 in maize. By analogy with defined mechanisms in the SL signaling network, a lack of SLs could attenuate transcriptional activity of TGA1 by sequestering its protein (together with that of NOT1) in SL-responsive complexes (Figure 7). When SL levels are low, TGA1 would bind to D53 (shown here) and be incorporated into a still larger SL-regulated complex with D14 (the SL receptor; also shown here). When D14 interacts with SL, it will recruit D3 (a director of SL-responsive ubiquitination), which will mediate SL-triggered breakdown of the entire complex. In maize, this release would allow TGA1 to form dimers that repress target genes (Figure 7), whereas the

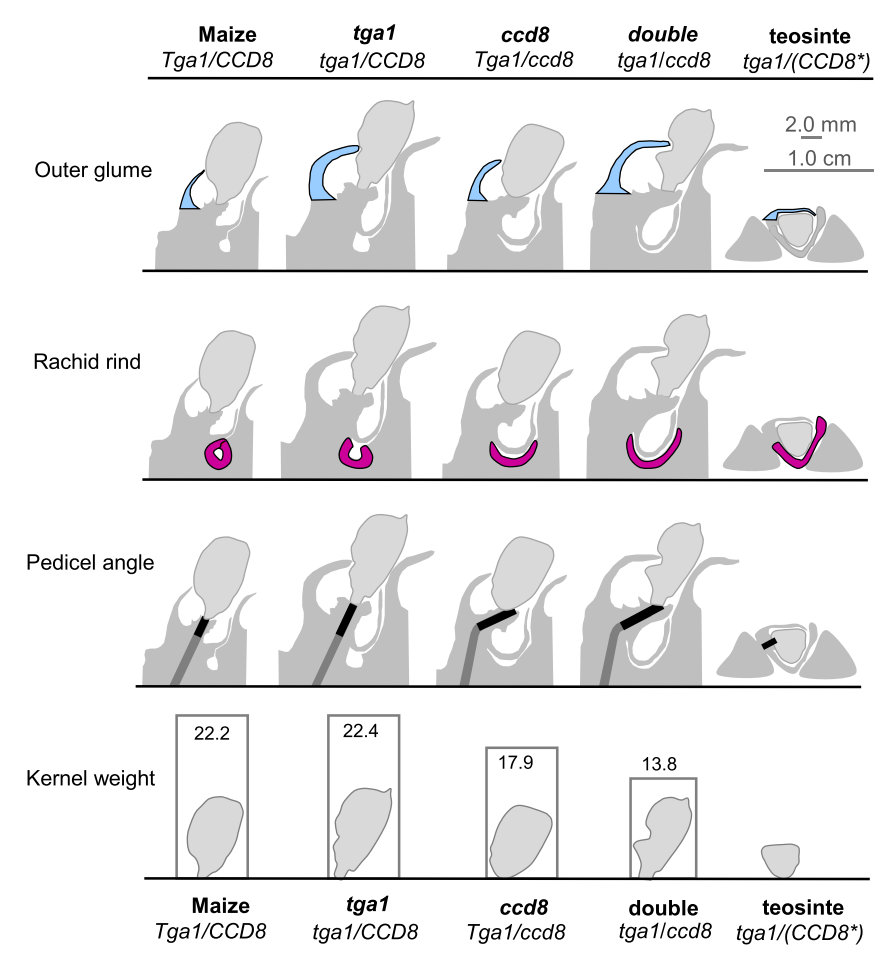


**Figure 10** Distinctive contributions by SLs and TGA1 are summarized visually alone and together to clarify their impacts on domestication phenotypes of grain-bearing cupules and kernels within them. Composite silhouettes of cupule and kernel architectures are shown for modern maize (TGA1/CCD8 in a W22 inbred), *tga1* (*tga1/CCD8*), *ccd8* (*TGA1/ccd8*), double recessive (*tga1/ccd8*), and teosinte (*tga1/CCD8*\*). Maternal profiles were taken directly from fresh sections most closely representing mean values for quantified structural parameters at 35 DAP, with mean cupule lengths measured as per Dorweiler and Doebley (1997). Kernel profiles were obtained similarly. All images are aligned relative to the deepest visible, adaxial point of each cupule. Outer glumes are shown in blue with black outline. Rachid rinds (magenta with black outline) are defined by visibly thickened layers of hypodermis lining the inner-cupule cavity. Pedicel shape, angles, and vascular tissues are in light gray, with dark gray highlighting altered angles between outer glumes and kernels. Seed weight and shape are presented in context with the cupules that bore them.

repression would be compromised in the absence of SLs (confirmed for *ccd8*), where TGA1 would remain sequestered with D53 and D14. Interestingly, this mechanistic signaling model predicts a phenotype like that of SL-deficient *ccd8* plants for lines where TGA1 levels are reduced by *RNAi* rather than sequestered by the SL signaling system (Wang et al, 2015). Reported similarities confirm this expectation and extend from prominent aspects of the vegetative plant to its shanks, tassels, ears and kernels (Figures 1 and 3, see also Wang et al., 2015). Together these results show how specific aspects of the S, L signaling network could modulate those of the TGA1 regulatory system in a manner consistent with their impact in maize and teosinte (Figure 7).

Three central features of this regulatory scenario differ between maize and its teosinte ancestor (Figure 7). The first is the well-defined contrast between teosinte *tga1* and its gain-of-function *Tga1* mutant in maize (Dorweiler et al.,

1993; Dorweiler and Doebley, 1997; Wang et al., 2005, 2015). Analyses indicate that a single amino-acid change (lysine to arginine) converts the maize TGA1 protein from a transcriptional activator to a homo-dimerizing repressor (Wang et al., 2005, 2015). The second difference arises from the first, because transcriptional repression by the maize TGA1 reduces the TGA1/NOT1 protein abundance by at least two-fold in maize relative to teosinte (Figure 6F and Preston et al., 2012; Wang et al, 2015). A third contrast between maize and teosinte is revealed here and lies not only in evidence for SL-regulation of the maize TGA1 transcription factor, but also in its independent control of additional domestication features in ear and kernel structure. The TGA1 signaling system would become SL-responsive when it converts from an activator in teosinte to a repressor in maize, where it would reduce levels of TGA1/NOT1 protein to such an extent that these would fall within range of control

by sequestration in the SL-regulated network. Selection for enhanced SL impact during maize improvement is consistent with the multifold elevated expression of the CCD8 gene for SL biosynthesis (two- to 10-fold depending on maize line, Figure 9A), as well as the SL-responsive phenotypic features observed earlier for vegetative architecture (Guan et al., 2012) and here for reproductive development (Figures 1, 3, 4, 6, and 10). In addition, domestication of maize took place in the New World where a selective advantage of elevated SLs would not have been impacted by associated susceptibility to Striga hermonthica, a parasitic plant that devastates maize yields in many parts of the globe.

Strigolactones-shaped ear evolution

Independent SL effects include striking alterations of the kernel-bearing cupules, particularly the shortening of rachid rinds and altered pedicel structure, whereas other impacts are consistent with evidence for an SL-responsive portion of the TGA1 network (Figure 10). Absence of SLs contributes characteristic features that, together with tga1, recapitulate the most primitive, teosinte-like grains and grain-bearing surfaces yet recovered. Key contributions by tga1 alone include elongation and in-curved growth of a teosinte-like outer glume and a partial uncurling of the rachid rind (Figure 10) as observed in previous work on this gene (Dorweiler et al., 1993; Dorweiler and Doebley, 1997; Wang et al., 2005, 2015). In contrast, specific impacts of low-SL status (as in ccd8) have a greater effect on unfolding of the rachid rind and enlargement of the cupule cavity. Shape and position of the pedicel are also converted to a primitive, teosinte-like angle when SLs are lacking. These changes demonstrate that both tga1 and ccd8, separately and together, mediate distinctive contributions to architecture of the grain-bearing surface, exposure of kernels on ears, and the size of resulting seeds.

Kernel size is a pivotally important domestication trait that increases multifold from teosinte to maize (Flint-Garcia et al., 2009; Figure 10). Although Tga1 is well known for its regulation of maternal seed-bearing structures, its full impact on grain size during domestication may have been underestimated (Wang et al., 2005). A clear role of TGA1 in kernel size is revealed here in an SL-deficient background (Figure 10) yet is lacking when examined in the high-SL state of modern maize (Figure 10 and previous studies [Dorweiler et al., 1993; Dorweiler and Doebley, 1997; Wang et al., 2005, 2015]). The absence of a kernel-size effect by Tga1 if SLs are abundant contrasts with the role of its rice ortholog, OsSPL16, in seed size, shape, and grain quality (Wang et al., 2012). Elevated expression of the wild-type OsSPL16 allele in rice promotes cell division and grain filling in high-yield varieties, whereas loss-of-function mutations lead to slender, high-quality grains like Basmati rice (Wang et al., 2012). Although results for maize are similar when RNAi is used to generate Tga1 loss-of-function mutants, these mutants do not parallel the unusual, native mutation in maize. Instead, the teosinte tga1 is converted from a transcriptional activator to a transcriptional repressor (TGA1) thus generating a gain-of-function rather than loss-of-function mutation. In addition, results here show that the seed-size effect of the

maize TGA1 is less than that of SLs (compare ccd8 and tga1 recessives to wild type [Figure 10]). The double recessive (tga1/ccd8) leads to a particularly small seed. This genetic combination also uncovers the presence of additional seedsize factors that are controlled independently by SLs. Collectively, these results indicate that SLs mediate grain size partially through Tga1 and that depletion of TGA1 protein by either RNAi (Wang et al., 2015) or sequestration by SL-responsive complexes (as inferred for ccd8) leads to an essentially identical small-seed phenotype (together with a full spectrum of ear and vegetative features [Figure 1 and Guan et al., 2012]). In addition, evidence extends beyond maize, since the prominent role of SLs in seed size is shown here to include other grains such as rice (Figure 1 and Table 1) and previously, tomatoes as well (Kohlen et al., 2012). These findings are further supported by analysis of the rice SL-deficient d10 (ccd8), d17 (ccd7), d27 (isomerase) and signaling-mutant d14 (SL receptor,  $\alpha/\beta$  fold hydrolase; Yamada et al., 2019).

A critical aspect of maize domestication is the coordination between seed size increase and changes in the grain-bearing surface. A prominent example is the protective effect of maternal tissues surrounding kernels, since we show here that these cupule structures can become detrimental if kernel growth is not controlled. In part, release of this restraint could occur if the proposed SL-regulation of TGA1 enhances retraction of maternal structures. However, the present work also shows that a more complete restructuring of the kernel-bearing surface and cupules involves additional, Tga1-independent impacts of SLs on ear architecture. These SL-mediated features include distinctive transitions of pedicel shape and cupule (rachid) structure that would further enhance kernel exposure, harvestability, and capacity for expansion. Comparisons in Figure 10 indicate that although Tga1 controls prominent changes in "teosinte glume architecture," SLs mediate a "teosinte rachid architecture." Concurrent regulation of seed size by SLs placed a critically important set of domestication traits under the umbrella of SL-coordination. We suggest that emergence of such a mechanism for dual control of kernel growth and cupule architecture would have been paramount during selection of modern-maize phenotypes. The SL-modulation of these features and related regulatory genes was apparently maintained during selection, where balance within this network would have been paramount.

### Materials and methods

### Plant materials and growth conditions

The W22 and B73 inbreds of maize (Zea mays ssp. mays L.) were used for wild-type and mutant genotypes compared in this study. The Ds insertion mutant of CCD8 (ccd8::Ds; W22 background) was developed by Vollbrecht et al. (2010) and initially characterized by Guan et al. (2012). The W22-tga1 line (W22 background) was developed by Dr. John Doebley and coworkers (Dorweiler et al., 1993), and provided through the Maize Genetics Coop Stock Center. Seeds of teosinte (Zea mays ssp. parviglumis H.H. Iltis & Doebley, accession: PI384061) were obtained through the North Central

Region Plant Introduction Station of the United States Department of Agriculture-Agricultural Research Service. The Ac-active line (Ac-immobilized, Ac::im; W22 background) was provided by the Boyce Thompson Institute (Ithaca, NY, USA; Vollbrecht et al., 2010). The Mutator (Mu) insertion lines of maize D53, D14a, and D14b (W22 background) were developed at the University of Florida from alleles initially created by the UniformMu (McCarty et al., 2013) and/or Mu-illumina (Williams-Carrier et al., 2010) groups. To minimize effects of hybrid vigor or additional Mu insertions in the mutant lines, all experimental material was backcrossed to the W22 inbred for at least 2 (UniformMu) or 5 (Mu-illumina) generations. Two near-isogenic lines (NILs) carrying teosinte alleles of CCD8 (Z033E0039 and Z031E0519; B73 background) were selected from the teosinte NIL set described in Liu et al. (2016). The polymerase chain reaction (PCR) genotyping primers used to distinguish the W22 TGA1 from the teosinte tga1 are listed Supplemental Data Set 3. Young seedlings of maize and teosinte were sampled after 14 days of growth in plastic containers of soil under controlled-chamber conditions at 24°C with photosynthetic active radiation (PAR) at 450 µmol m<sup>-2</sup> s<sup>-1</sup> and a 16/8-h light/dark cycle. Greenhouse-grown materials were used for string-feeding experiments and field-grown plants for developmental analyses of plant morphology and ears. The University of Florida research farm (Plant Science Research and Education Unit) is located at Citra, FL, USA.

# Genetic crosses and screening for development of a ccd8::Ds revertant (CCD8::Rev)

A population for this mutant screen was developed by crossing the homozygous Activator (Ac)-inactive ccd8::Ds mutant with the Ac::im line (Vollbrecht et al., 2010). The  $F_1$  plants were self-pollinated to produce  $F_2$  seeds. The  $F_2$  plants that segregated for both homozygous ccd8::Ds and Ac activity were again self-pollinated to produce  $F_3$  kernels. A revertant (CCD8::Rev) was identified from approximately 1,200 of these  $F_3$  seedlings by screening for the solid green leaves that lacked yellow stripes typical of the ccd8 phenotype. The revertant genotype was verified by PCR and sequence analysis. Primers used for PCR genotyping are listed in Supplemental Data Set 3. The revertant was self-pollinated and its ear and plant phenotypes were characterized at the  $F_4$  and  $F_5$  generations.

# Complementation of the revertant CCD8 allele (CCD8<sup>R426G</sup>) in an Arabidopsis *max4-6* mutant

To generate the construct for complementation analysis in Arabidopsis, the maize *CCD8* coding region was first subcloned between the restriction sites *BamH* I and *EcoR* I of the pGEX-2 T vector. The C nucleotide at the 1,276th position of the *CCD8* coding sequence in maize was then replaced with a G nucleotide by using the Q5 Site-Directed Mutagenesis kit (NEB, Ipswich, MA, USA) according to the manufacturer's instructions. After confirming the change by Sanger sequencing, the *CCD8*<sup>R426G</sup> coding region was

amplified by PCR and then subcloned between the Spe I and BstE II sites of the pCAMBIA1305.1 vector placing it downstream of the cauliflower mosaic virus (CaMV) 35S promoter. The primers used for cloning are listed in Supplemental Data Set 3. The constructs were transformed into Agrobacterium tumefaciens strain GV3101 and used for transforming Arabidopsis max4-6 via floral dip (Clough and Bent, 1998). The  $T_0$  seeds were selected on culture plates with hygromycin (30 μg mL<sup>-1</sup>) in half-strength MS. Surviving seedlings were transferred to soil and grown in germination mix (Sun-Gro) under controlled conditions at 22°C and PAR at 150 μmol m<sup>-2</sup> s<sup>-1</sup> with a 16/8-h light/dark cycle. The wild-type (Col-0) control and max4-6 seeds were germinated without antibiotics under the same culture conditions. The number of rosette branches on all seedlings was recorded at 3 weeks after flowering. For expression analyses, leaves from each independent line were harvested at 3 weeks after planting. Total RNA was extracted from leaves and purified using the plant RNeasy kit (Qiagen, Valencia, CA, USA). Concentration of RNA was determined spectrophotometrically with a NanoDrop 1000 (Thermo Fisher Scientific). Genomic DNA was removed with RQ1 RNase-free DNase (Promega, Madison, WI, USA). To quantify expression of CCD8<sup>R426G</sup> in transgenic plants, 50 µg total RNA were used in the SuperScript III One-Step reverse transcription (RT)-PCR system (Invitrogen, Carlsbad, CA, USA). The Arabidopsis Tubulin gene provided an internal control. Primers used for RT-PCR analyses are listed in Supplemental Data Set 3.

### String-feeding system

To test if the cupule enlargement observed in ccd8 ears was due to SL deficiency, the synthetic SL analog, GR24, was delivered into greenhouse-grown mutant and wild-type plants. The GR24 was obtained and prepared as described in our previous work (Guan et al., 2012). Mercerized cotton thread (size 3) and a sewing needle were purchased from a local vendor (Walmart). When plants reached the 11-leaf stage of development, the first set of cotton wicking threads were inserted. The needle was used to guide each thread through the fourth internode of the stem and then through the cap of a 2-mL microcentrifuge tube. A knot was tied inside the cap and the remaining thread immersed in a solution of either 1 μM GR24 or 0.02% (v/v) DMSO (the solvent used for GR24). The other end of the wicking thread was treated similarly prior to sealing the caps by snapping their lids. Two threads were used for the first wicking system of each individual plant. Two weeks later, another two threads were used to set up the second wicking system at the internode just below that of the ear. The level of solution was checked twice per day during the first few days, then once per day. Solutions were replenished as needed and treatments were continued until ears were ready for harvest.

### Comparison of ear phenotypes

Architecture of ears and cupules was quantified using methods established previously for domestication features of tga1

mutants (Guan et al., 2012). The cupule length (rachis internode), outer-glume thickness, and outer-glume length were measured at 21 days-after-pollination (DAP). All analyses were done using spikelets in the fourth to sixth positions from the base of the ear. Cupule length was determined by measuring the total length of 8-10 consecutive internodes starting near the base of the ear and then dividing by that number to get the average cupule length. Student's t test (Excel, Microsoft) was used to test for statistically significant differences between the ccd8 mutants and normal wild-type siblings.

### Histological analysis

Strigolactones-shaped ear evolution

Ears of field-grown plants were harvested at 10 days postpollination (summer 2013), dissected, and vacuum-infiltrated with FAA (3.7% (v/v)) formaldehyde, 5% (v/v) acetic acid and 50% (v/v)v) ethanol). Samples were dehydrated through an ethanol series, treated with Histoclear (Thermo Scientifc), and embedded in Paraplast (Thermo Scientifc). Sectioning (4 µm) was done using protocols at the Molecular Pathology Core (Dept. of Pathology, Immunology and Lab. Medicine, University of Florida) followed by Hematoxylin and Eosin (H&E; Thermo Scientifc) staining. Brightfield scanning (Aperio Scanscope CS) was used for image acquisition and ImageScope software (Aperio) for viewing and analysis.

### Molecular analysis of CCD8 alleles in maize and teosinte

The seeds of teosinte inbreds were kindly provided by Dr. John Doebley. For preparation of genomic DNA, leaf tissues ( $\sim$  0.1 g) were ground first in liquid nitrogen, then extracted in 0.5-mL DNA extraction buffer (6.93 M urea, 50 mM Tris-HCl [pH 8.0], 0.3125 mM NaCl, 20 mM EDTA [pH 8.0], and 1% [w/v] SDS). The genomic DNA fragment containing CCD8 was amplified with the primer pair for CCD8-Fw-2 and either CCD8-Rv-2 or CCD8-Rv-3 (Supplemental Data Set 3) using the Phusion Green Hot Start II High-Fidelity PCR Master Mix (Thermo Scientific). The PCR products were purified after gel elution using the Agarose Dissolving Buffer (ADB; Zymo Research, Irvine, CA, USA) and verified by Sanger sequencing (GENEWIZ). Nucleotide sequences were aligned using the Clustal Omega program (https:// www.ebi.ac.uk/Tools/msa/clustalo/). To calculate differences in the nucleotide diversity between maize and teosinte in the CCD8 genomic region, we used the "Diversity" program in the MaizeSNPDB database (http://150.109.59.144:3838/ MaizeSNPDB/; Zhou et al., 2019). The genotype database contains 1,111 improved maize lines, 25 maize landraces, 20 teosinte lines, and 54 other maize lines. Each sliding window contains five SNP sites. There are 179 SNPs across 15 kb upstream and downstream of the CCD8 genomic region.

### RNA-seq profiling and analysis

Juvenile ears (~2.5 cm) were harvested from plants grown under controlled-chamber conditions of 24°C with PAR at 450  $\mu$ mol m<sup>-2</sup> s<sup>-1</sup> and a 16/8-h light/dark cycle. Three

biological replicates were sampled from each genotype and total RNA was extracted using RNeasy Plant Mini Kits (QIAGEN). Transcript quality was verified with a Bioanalyzer (Agilent) at the UF-ICBR (Interdisciplinary Center for Biotechnological Research) core facility. Each sublibrary for multiplexing was constructed from 1 µg of total RNA from each sample. Individual sublibraries were generated using TruSeq Stranded Total RNA Sample Preparation Kit with Ribo-Zero Plant (Illumina). For quality control analysis, the quality and quantity of sublibraries was checked with the Bioanalyzer as noted above. The DNA library templates were quantified by qPCR with KAPA Library Quantification Kits (KAPA BIOSYSTEMS) following manufacturer's instructions. Libraries were multiplexed, then sequenced using NexSeq500 (Illumina; instrument at the UF-ICBR core facility). Data from RNA-seq were analyzed using the Tuxedo suite in the Galaxy platform hosted at UF Research Computing (Goecks et al., 2010). The read alignment workflow progressed from fastq groomer to fastq QC, fastq trimmer, then Tophat2 (Trapnell et al., 2012). Parameters were adjusted for read lengths (typically about 150 bp for NexSeq500). Default settings were otherwise used. Differentially expressed genes (DEGs) were identified by Cuffdiff (Trapnell et al., 2012).

### Gene expression analysis by quantitative real-time **RT-PCR**

Total RNA was isolated from immature ears (2.3–2.8 cm in length to ensure developmentally equivalent samples) and root systems of 14-day-old seedlings using the plant RNeasy kit (Qiagen). Tissues were ground in liquid nitrogen and half the resulting powder from each sample was kept for protein extraction. Concentration of RNA was determined using a NanoDrop 1000 spectrophotometer (Thermo Scientific). Total RNA from each sample was treated with the RQ1 RNase-free DNase (Promega) to remove traces of genomic DNA. For quantitative RT-PCR, the Power SYBR green RNA-to-C<sub>t</sub> 1-step kit (Applied Biosystems) was used with an iCycler iQ real-time PCR detection system (Bio-rad). For absolute quantification, the gene-specific DNA fragments used as standards were amplified by PCR. Resulting products were purified after gel elution, their concentrations determined using a NanoDrop 1000 spectrophotometer (Thermo Scientific), and their identity verified by Sanger sequencing. The copy number per nanogram of fragment was then determined to establish a standard curve. For analysis of CCD8 expression, DNA fragments were amplified using W06.1407-F1 and W06.1407-R1 as primer pairs (Supplemental Data Set 3). For quantitative RT-PCR, CCD8-qRT-F3 and CCD8-qRT-R3 were used (Supplemental Data Set 3). For analysis of TGA1 and NOT1 expression, primer pairs were adapted from Preston et al. (2012). The primers for TGA1 were Tga1-qRT-F and Tga1-qRT-R (Supplemental Data Set 3), and those for NOT1 were Not1-qRT-F and Not1-qRT-R (Supplemental Data Set 3).

### Immunoblot analysis

Powdered samples of the immature ears described previously were used for protein extraction using a Plant Total Protein

Extraction kit (Sigma, Saint Louis, MO, USA) as described by Wang et al. (2005). Protein concentrations were determined using the Bradford dye reagent (Bio-Rad, Hercules, CA, USA) and purified BSA (Bio-Rad) as a standard. For immunoblotting, 25 µg of protein from each sample was loaded onto a precast TGX stain-free AnyKD gel (Bio-Rad), separated, and transferred to the Sequi-blot PVDF membrane (Bio-Rad) using the Trans-blot SD Semi-Dry transfer cell (Bio-Rad). To block nonspecific sites, the membrane was incubated in a shaking solution of 1× TBS and 1% casein blocker (Bio-Rad) at room temperature for at least 1 h. The blot was then probed with anti-TGA1 primary antibody (1:1,000 dilution; kindly provided by Dr. John Doebley) and anti-actin (I-19)-R (sc-1616) antibody (1:1,000 dilution; Lot # G0312; Santa Cruz Biotechnology, Santa Cru, CA, USA). Actin level provided a loading control as described by Wang et al. (2005). The HRP-conjugated goat anti-rabbit secondary antibody (1:10,000 dilution; Lot# DF720699, Pierce, Rockford, IL, USA) was used to recognize primary antibodies. The Clarity western ECL substrate (Bio-Rad) was used to visualize HRP on the blot and the chemiluminescent signal was imaged by a CCD camera system (Bio-Rad). Signal strength on the immunoblot was quantified with ImageJ software.

### Y2H assays

The Matchmaker Gold Yeast Two-Hybrid System (Takara, Mountain View, CA, USA) was used to test potential protein-protein interactions. Total RNA from immature ears provided templates for cDNA synthesis and PCR amplification of coding sequences of Tga1 and the maize genes for D53a and D14a. The Superscript III One-Step High-Fidelity RT-PCR kit (Invitrogen) was used for this purpose. Primers for vector construction are listed in Supplemental Data Set 3. The RT-PCR products were cloned into a pCR4 TOPO TA cloning vector (Invitrogen). Plasmids were prepared using a Zyppy Plasmid Miniprep kit (Zymo Research, Irvine, CA, USA) and the nucleotide sequence of each cDNA clone was verified by Sanger sequencing. Validated plasmids provided templates for PCR amplification of DNA fragments to construct Y2H vectors. The coding sequences of each full-length, deleted, or truncated TGA1 were separately cloned into the site between EcoR I and BamH I for fusion in frame with the GAL4 AD in the pGADT7 vector. In contrast, the coding sequence of maize D53a was cloned into the site between EcoR I and BamH I for fusion in frame with the GAL4 DNA-BD of the pGBKT7 vector. For the 7 aa, truncated TGA1 (pGADT7:TGA1 $^{\Delta7}$ ), we first cloned the coding sequence of TGA1 into the site between Bam HI and Eco RI of the pGEX-2T vector to obtain pGEX-2T-TGA1. The residues from positions 172 to 178 (HNRRRPK) of TGA1 were then truncated from the pGEX-2T-TGA1 using a Q5 Site-Directed Mutagenesis kit (NEB, Ipswich, MA, USA). The resulting pGEX-2T-TGA1 $^{\Delta7}$  construct provided the template for cloning into the pGADT7 vector. The DNA fragments were amplified using the Phusion Green Hot Start High-Fidelity DNA polymerase (Thermo Scientific). After restriction enzyme treatment (NEB), fragments were purified using Zymoclean DNA Recovery kit (Zymo Research). For ligations, purified DNA fragments were joined to linearized vectors using a Quick Ligation kit (NEB). Ligated products were transformed into the NEB 5-α Competent E. coli (NEB). After verifying nucleotide sequences of each construct by Sanger sequencing, pGADT7-TGA1 and pGBKT7-D53a constructs were co-transformed into the Y2HGOLD yeast strain (Saccharomyces cerevisiae) using the Frozen-EZ Transformation II kit (Zymo Research). Transformed yeast cells were plated on selection medium without leucine or tryptophan (double dropout selection medium, DDO: -LT) or on selection medium without adenine, histidine, leucine or tryptophan (quadruple dropout selection medium, QDO: -LTHA) containing 40  $\mu$ g mL<sup>-1</sup> X- $\alpha$ -Gal and 125 ng mL<sup>-1</sup> aureobasidin A at 30°C for 3–5 days. For clarity, the positive colony (1 $\sim$ 2 mm in diameter) was harvested, suspended in 50-µL sterile water, and 1-µL of the resulting cell suspension spotted on the selection medium as indicated. Colonies were imaged after incubation at 30°C for 2~3 days. A Known affinity between p53 and the large T-antigen (T) provided a positive control for interactions, and a noninteracting lamin (Lam) was used with the T-antigen for a negative control.

### BiFC assays and confocal microscopy

For assessment of in vivo protein-protein interactions, we used a Double ORF Expression BiFC system (pDOE), which has a high signal-to-noise ratio and a significant reduction of nonspecific assembly (Gookin and Assmann, 2014). To fuse with the 210-amino-acid N terminus of monomeric Venus florescent protein (NmVen210) in the pDOE-06 vector, the coding sequences of full-length TGA1, or truncated TGA1 (TGA1<sup>Δ7</sup>) were separately cloned into the MCS1 restriction sites between Spe I and BamH I. Resulting constructs were designated pDOE-06-TGA1:NmVen and pDOE-06-TGA1<sup>Δ7</sup>:NmVen. For testing the interaction between TGA1 and the maize D53, the coding sequence of D53 was cloned into the Pml I site in the MCS3 of either pDOE-06, pDOE-06-TGA1:NmVen, or pDOE-06-TGA1 $^{\Delta7}$ :NmVen. The resulting constructs were pDOE-06-D53:CVen, pDOE-06-TGA1:NmVen-D53:CVen and pDOE-06-TGA1<sup>Δ7</sup>:NmVen-D53:CVen. The coding sequence of D14a was cloned into the sites between San DI and Pml I in the MCS3 of pDOE-05 vector to construct pDOE-05-D14a: Cven. In this arrangement, interaction between D53 and D14a will prevent assembly of a functional florescent protein. All constructs were verified by Sanger sequencing (GENEWIZ). Each construct was introduced into Agarobacterium tumefaciens strain GV3101 by electroporation (Bio-rad) and selected on YM agar plates supplemented with 50 µg mL<sup>-1</sup> kanamycin and 15 μg mL<sup>-1</sup> gentamicin. After incubation at 30°C for 2-3 days, one colony were inoculated into LB medium with  $50 \, \mu g \, mL^{-1} \,$  kanamycin,  $15 \, \mu g \, mL^{-1} \,$  gentamicin and  $100 \, \mu M$ acetosyringone (Sigma-Aldrich) at 30°C and incubated overnight. Cells were pelleted and resuspended in infiltration buffer (10 mM MES, 10 mM MgCl<sub>2</sub>, pH 5.6 with KOH, 100 μM acetosyringone). Cell concentrations were adjusted to 0.2 (OD<sub>600</sub>) and the final concentration for infiltration was 0.1 (OD<sub>600</sub>) for each vector. Nicotiana benthamiana plants were grown in germination mix (Sun-Gro) under controlled-chamber conditions at 22°C with PAR at 150 µmol m<sup>-2</sup> s<sup>-1</sup>, and a 12-h light/dark cycle. Each set of multiple infiltrations was tested on a single leaf at the fifth to seventh position on an N. benthamiana plant at the nine-leaf stage. Experiments were replicated three times, with each replicate involving leaves on at least three different plants. To quantify the effects of different constructs on leaf necrosis or senescence, the chlorophyll contents or "greenness" of leaves were determined by a SPAD 502 Chlorophyll Meter (Spectrum Technologies, Plainfield, IL) at 6 days after infiltration. SPAD values are defined by Konica Minolta as indicators of relative chlorophyll levels present in plant tissues. Subcellular imaging was done with a Leica TCS SP5 confocal microscope at light wavelength and parameters described by Gookin and Assmann (2014).

### **Quantification of SLs**

Individual two-week-old seedlings were each cultured in 50-mL Falcon tubes and grown under conditions described by Charnikhova et al. (2017, 2018). Detection and measurement of SLs in root exudates was conducted as described previously (Charnikova et al. 2017, 2018). Zealactone was quantified by calculating the area under the LC-MS/MS peak at m/z 377 > 97.

### Statistical analysis

Microsoft Excel (2016) or the Online Web Statistical Calculators (astatsa.com) was used for statistical tests. The comparison of sample means was done by the Student's t test or the one-way analysis of variance (ANOVA) followed by Tukey HSD (Honestly Significant Difference) test. The results of statistical analysis are shown in Supplemental Data Set 4.

### **Accession numbers**

Sequence data from this article can be found in the EMBL/ GenBank data libraries under accession numbers: CCD8 (Zm00001d043442), D3a (Zm00001d045313), D14a (Zm00001d028294), D14b (Zm00001d048146), D53 (Zm00001d023208), TGA1 (GRMZM2G101511), NOT1 (Zm00001d049824). RNA-seq data are available at the National Center for Biotechnology Information Gene Expression Omnibus (http://www.ncbi.nlm.nih.gov/geo) under the accession PRJNA854162.

### Supplemental data

The following materials are available in the online version of this article.

**Supplemental Figure S1.** Diagrams of maize *D14a* and *D14b* gene structure along with the location of each transposon insertion.

**Supplemental Figure S2.** Confocal micrographs of combinations of different constructs.

**Supplemental Figure S3.** Nucleotide sequence analysis of *ZmCCD8* alleles in sub-species of *Zea mays*.

**Supplemental Table S1.** Numbers of branches at 3 weeks after flowering by *Arabidopsis* were consistently greater for individual *max4*–6 (transgenic *ZmCCD8*) plants than for Col-0 (wild type).

**Supplemental Data Set S1**. Genes co-regulated by *Tga1* and SL signaling.

**Supplemental Data Set S2.** Maize domestication and improvement candidate genes regulated by strigolactones in immature ears (2.5 to 3.0 cm).

**Supplemental Data Set S3.** Primer list for cloning, genotyping, and gene expression analysis.

Supplemental Data Set S4. Details of statistical analyses.

### Acknowledgments

We thank Dr. John Doebley (Department of Genetics, University of Wisconsin-Madison) for providing the TGA1 antibody and Dr. Lincoln Zotarelli (Horticultural Sciences Department, University of Florida) for the SPAD chlorophyll meter. This work was supported by the National Science Foundation, USA under grants: NSF-IOS-PGRP-1521100 (to J.-C.G. and K.E.K.), NSF-IOS-PGRP-1025976 (to K.E.K.), NSF-IOS-PGRP-1116561 (to D.R.M. and K.E.K.), and NSF-IOS-PGRP-1748105 (to D.R.M. and K.E.K.); the European Research Council (ERC) Advanced grant CHEMCOMRHIZO (670211; to H.J.B.); Marie Curie fellowship NEMHATCH (793795; to L.D.); and China Scholarship Council (CSC) scholarship (to C.L.).

Conflict of interest statement. The authors declare no conflict of interest.

### References

**Al-Babili S, Bouwmeester HJ** (2015) Strigolactones, a novel carotenoid-derived plant hormone. Annu Rev Plant Biol **66**(1): 161–186

Aliche EB, Screpanti C, De Mesmaeker A, Munnik T, Bouwmeester HJ (2020) Science and application of strigolactones. New Phytol 227(4): 1001–1011

Beadle GW (1979) The ancestry of corn. Sci Am 242(1): 112-119

Bertheloot J, Barbier F, Boudon F, Perez-Garcia M D, Péron T, Citerne S, Dun E, Beveridge C, Godin C, Sakr S (2020) Sugar availability suppresses the auxin-induced strigolactone pathway to promote bud outgrowth. New Phytol 225(2): 866–879

**Bürger M, Chory J** (2020) The many models of strigolactone signaling. Trends Plant Sci **25**(4): 395–405

Cardoso C, Zhang Y, Jamil M, Hepworth J, Charnikhova T, Dimkpa SO, Meharg C, Wright MH, Liu J, Meng X, et al. (2014) Natural variation of rice strigolactone biosynthesis is associated with the deletion of two MAX1 orthologs. Proc Natl Acad Sci USA 111(6): 2379–2384

Charnikhova TV, Gaus K, Lumbroso A, Sanders M, Vincken JP, De Mesmaeker A, Ruyter-Spira CP, Screpanti C, Bouwmeester HJ (2017) Zealactones. Novel natural strigolactones from maize. Phytochem 137(May): 123–131

Charnikhova TV, Gaus K, Lumbroso A, Sanders M, Vincken JP, De Mesmaeker A, Ruyter-Spira CP, Screpanti C, Bouwmeester HJ

- (2018) Zeapyranolactone A novel strigolactone from maize. Phytochem Lett **24**(April): 172–178
- Chesterfield RJ, Vickers CE, Beveridge CA (2020) Translation of strigolactones from plant hormone to agriculture: achievements, future perspectives, and challenges. Trends Plant Sci 25(11): 1087–1106
- Chuck G, Brown PJ, Meeley R, Hake S (2014) Maize SBP-box transcription factors unbranched2 and unbranched3 affect yield traits by regulating the rate of lateral primordia initiation. Proc Natl Acad Sci USA 111(52): 18775–18780
- Chuck G, Cigan AM, Saeteurn K, Hake S (2007) The heterochronic maize mutant *Corngrass1* results from overexpression of a tandem microRNA. Nat Genet **39**(4): 544–549
- Chuck G, Whipple C, Jackson D, Hake S (2010) The maize SBP-box transcription factor encoded by *tasselsheath4* regulates bract development and the establishment of meristem boundaries. Development **137**(8): 1243–1250
- **Clough SJ, Bent AF** (1998) Floral dip: a simplified method for *Agrobacterium*-mediated transformation of *Arabidopsis thaliana*. Plant J **16**(6): 735–743
- **Doebley J** (2004) The genetics of maize evolution. Ann Rev Genet **38**(1): 37–59
- Doll NM, Depège-Fargeix N, Rogowsky PM, Widiez T (2017) Signaling in early maize kernel development. Mol Plant 10: 375-388
- Dong Z, Xiao Y, Govindarajulu R, Feil R, Siddoway ML, Nielsen T, Lunn JE, Hawkins J, Whipple C, Chuck G (2019) The regulatory landscape of a core maize domestication module controlling bud dormancy and growth repression. Nat Commun 10: 3810
- **Dorweiler JE, Doebley JF** (1997) Developmental analysis of *teosinte* glume architecture1: a key locus in the evolution of maize (*Poaceae*). Am J Bot **84**(10): 1313–1322
- **Dorweiler J, Stec A, Kermicle J, Doebley J** (1993) *Teosinte glume architecture* 1: a genetic locus controlling a key step in maize evolution. Science **262**(5131): 233–235
- Flint-Garcia SH, Bodnar AL, Scott MP (2009) Wide variability in kernel composition, seed characteristics, and zein profiles among diverse maize inbreds, landraces, and teosinte. Theor Appl Genet 119(6): 1129–1142
- Goecks J, Nekrutenko A, Taylor J (2010) The galaxy team. Galaxy: a comprehensive approach for supporting accessible, reproducible, and transparent computational research in the life sciences. Genome Biol 11(8): R86
- Gomez-Roldan V, Fermas S, Brewer PB, Puech-Pagès V, Dun EA, Pillot JP, Letisse F, Matusova R, Danoun S, Portais JC, et al. (2008) Strigolactone inhibition of shoot branching. Nature 455(7210): 189–194
- Gookin TE, Assmann SM (2014) Significant reduction of BiFC non-specific assembly facilitates in planta assessment of heterotrimeric G-protein interactors. Plant J 80(3): 553–567
- Guan JC, Koch KE, Suzuki M, Wu S, Latshaw S, Petruff T, Goulet C, Klee HJ, McCarty DR (2012) Diverse roles of strigolactone signaling in maize architecture and the uncoupling of a branching-specific subnetwork. Plant Physiol 160(3): 1303–1317
- Hufford MB, Xu X, van Heerwaarden J, Pyhäjärvi T, Chia JM, Cartwright RA, Elshire RJ, Glaubitz JC, Guill KE, Kaeppler SM, et al. (2012) Comparative population genomics of maize domestication and improvement. Nat Genet 44(7): 808–811
- Ishikawa S, Maekawa M, Arite T, Onishi K, Takamure I, Kyozuka J (2005) Suppression of tiller bud activity in *tillering dwarf* mutants of rice. Plant Cell Physiol **46**(1): 79–86
- Jamil M, Charnikhova T, Houshyani B, van Ast A, Bouwmeester HJ (2012) Genetic variation in strigolactone production and tillering in rice and its effect on Striga hermonthica infection. Planta 235(3): 473–484
- Jiang L, Liu X, Xiong G, Liu H, Chen F, Wang L, Meng X, Liu G, Yu H, Yuan Y, et al. (2013) DWARF 53 Acts as a repressor of strigolactone signalling in rice. Nature 504(7480): 401–405
- Jiao Y, Wang Y, Xue D, Wang J, Yan M, Liu G, Dong G, Zeng D, Lu Z, Zhu X, et al. (2010) Regulation of OsSPL14 by OsmiR156 defines ideal plant architecture in rice. Nat Genet 42(6): 541–544

- Koch K, Ma F (2017) Maize kernel development, Chapter 15. Brian A. Larkins, pp. 190–203
- Kohlen W, Charnikhova T, Lammers M, Pollina T, Tóth P, Haider I, Pozo MJ, de Maagd RA, Ruyter-Spira C, Bouwmeester HJ, et al. (2012) The tomato CAROTENOID CLEAVAGE DIOXYGENASE8 (SICCD8) regulates rhizosphere signaling, plant architecture and affects reproductive development through strigolactone biosynthesis. New Phytol 196(2): 535–547
- Liu Z, Cook J, Melia-Hancock S, Guill K, Bottoms C, Garcia A, Ott O, Nelson R, Recker J, Balint-Kurti P, et al. (2016) Expanding maize genetic resources with predomestication alleles: maize—teosinte introgression populations. Plant Genome 9(1): plantgenome2015.07.0053.
- Liu J, Novero M, Charnikhova T, Ferrandino A, Schubert A, Ruyter-Spira C, Bonfante P, Lovisolo C, Bouwmeester HJ, Cardinale F (2013) CAROTENOID CLEAVAGE DIOXYGENASE 7 modulates plant growth, reproduction, senescence, and determinate nodulation in the model legume Lotus japonicus. J Exp Bot 64(7): 1967–1981
- Liu Y, Wu G, Zhao Y, Wang HH, Dai Z, Xue W, Yang J, Wei H, Shen R, Wang H (2021) DWARF53 Interacts with transcription factors UB2/UB3/TSH4 to regulate maize tillering and tassel branching. Plant Physiol 187(2): 947–962
- Matsuoka Y, Vigouroux Y, Goodman MM, Sanchez JG, Buckler E, Doebley J (2002) A single domestication for maize shown by multilocus microsatellite genotyping. Proc Natl Acad Sci USA 99(9): 6080–6084
- McCarty DR, Latshaw S, Wu S, Suzuki M, Hunter CT, Avigne WT, Koch KE (2013) Mu-seq: sequence-based mapping and identification of transposon induced mutations. PLoS One 8(10): e77172
- Miura K, Ikeda M, Matsubara A, Song XJ, Ito M, Asano K, Matsuoka M, Kitano H, Ashikari M (2010) OsSPL14 promotes panicle branching and higher grain productivity in rice. Nat Genet 42(6): 545–549
- Moreno M, Haper LC, Krueger RW, Dellaporta SL, Freeling M (1997) Liguleless1 encodes a nuclear-localized protein required for induction of ligules and auricles during maize leaf organogenesis. Genes Dev 11(5): 616–628
- Pasare SA, Ducreux LJM, Morris WL, Campbell R, Sharma SK, Roumeliotis E, Kohlen W, van der Krol S, Bramley PM, Roberts AG, et al. (2013) The role of the potato (Solanum tuberosum) CCD8 gene in stolon and tuber development. New Phytol 198(4): 1108–1120
- Piperno DR, Ranere AJ, Holst I, Iriarte J, Dickau R (2009) Starch grain and phytolith evidence for early ninth millennium B.P. Maize from the central Balsas river valley, Mexico. Proc Natl Acad Sci USA 106(13): 5019–5024
- Preston JC, Wang H, Kursel L, Doebley J, Kellogg EA (2012) The role of teosinte glume architecture1 (tga1) in coordinated regulation and evolution of grass glumes and inflorescence axes. New Phytol 193(1): 204–215
- Ramos-Madrigal J, Smith BD, Moreno-Mayar JV, Gopalakrishnan S, Ross-Ibarra J, Gilbert MTP, Wales N (2016) Genome sequence of a 5,310-year-old maize cob provides insights into the early stages of maize domestication. Curr Biol 26(23): 3195–3201
- Ravazzolo L, Trevisan S, Manoli A, Boutet-Mercey SP, Perreau FO, Quaggiotti S (2019) The control of zealactone biosynthesis and exudation is involved in the response to nitrogen in maize root. Plant Cell Physiol 60(9): 2100–2112
- Roesler K, Lu C, Thomas J, Xu Q, Vance P, Hou Z, Williams RW, Liu L, Owens MA, Habben JE (2021) Arabidopsis carboxylesterase 20 binds strigolactone and decreases branches and tillers when extopically expressed in Arabidopsis and maize. Front Plant Sci 12(April): 639401
- Sang D, Chen D, Liu G, Liang Y, Huang L, Meng X, Chu J, Sun X, Dong G, Yuan Y, et al. (2014) Strigolactones regulate rice tiller angle by attenuating shoot gravitropism through inhibiting auxin biosynthesis. Proc Natl Acad Sci USA 111(30): 11199–11204
- Sekhon RS, Lin H, Childs KL, Hansey CN, Buell CR, de Leon N, Kaeppler SM (2011) Genome-wide atlas of transcription during maize development. Plant J 66(4): 553–563
- Song X, Lu Z, Yu H, Shao G, Xiong J, Meng X, Jing Y, Liu G, Xiong G, Duan J, et al. (2017) IPA1 Functions as a downstream transcription factor repressed by D53 in strigolactone signaling in rice. Cell Res 27(9): 1128–1141

- Trapnell C, Roberts A, Goff L, Pertea G, Kim D, Kelley DR, Pimentel H, Salzberg SL, Rinn JL, Pachter L (2012) Differential gene and transcript expression analysis of RNA-seq experiments with TopHat and cufflinks. Nat Protoc **7**(3): 562–578
- Umehara M, Hanada A, Yoshida S, Akiyama K, Arite T, Takeda-Kamiya N, Magome H, Kamiya Y, Shirasu K, Yoneyama K, et al. (2008) Inhibition of shoot branching by new terpenoid plant hormones. Nature 455(7210): 195–200
- Vollbrecht E, Duvick J, Schares JP, Ahern KR, Deewatthanawong P, Xu L, Conrad LJ, Kikuchi K, Kubinec TA, Hall BD, et al. (2010) Genome-wide distribution of transposed dissociation elements in maize. Plant Cell 22(6): 1667–1685
- Wang H, Nussbaum-Wagler T, Li B, Zhao Q, Vigouroux Y, Faller M, Bomblies K, Lukens L, Doebley JF (2005) The origin of the naked grains of maize. Nature **436**(7051): 714–719
- Wang Y, Shang L, Yu H, Zeng L, Hu J, Ni S, Rao Y, Li S, Chu J, Meng X, et al. (2020) A strigolactone biosynthesis gene contributed to the green revolution in rice. Mol Plant 13(6): 923–932
- Wang H, Studer AJ, Zhao Q, Meeley R, Doebley JF (2015) Evidence that the origin of naked kernels during maize domestication was caused by a single amino acid substitution in *tga1*. Genetics **200**(3): 965–974
- Wang S, Wu K, Yuan Q, Liu X, Liu Z, Lin X, Zeng R, Zhu H, Dong G, Qian Q, et al. (2012) Control of grain size, shape and quality by OsSPL16 in rice. Nat Genet 44(8): 950-954
- Williams-Carrier R, Stiffler N, Belcher S, Kroeger T, Stern DB, Monde RA, Coalter R, Barkan A (2010) Use of illumina sequencing to identify transposon insertions underlying mutant phenotypes in high-copy *Mutator* lines of maize. Plant J **63**(1): 167–177
- Xie X, Kisugi T, Yoneyama K, Nomura T, Akiyama K, Uchida K, Yokota T, McErlean CSP, Yoneyama K (2017) Methyl zealactonoate, a novel

- germination stimulant for root parasitic weeds produced by maize. J Pestic Sci **42**(2): 58–61
- Xu E, Chai L, Zhang S, Yu R, Zhang X, Xu C, Hu Y (2021) Catabolism of strigolactones by a carboxylesterase. Nat Plants 7(11): 1495–1504
- Yamada Y, Otake M, Furukawa T, Shindo M, Shimomura K, Yamaguchi S, Umehara M (2019) Effects of strigolactones on grain yield and seed development in rice. J Plant Growth Regul 38(3): 753-764
- Yoneyama K, Akiyama K, Brewer PB, Mori N, Kawano-Kawada M, Haruta S, Nishiwaki H, Yamauchi S, Xie X, Umehara M, et al. (2020) Hydroxyl carlactone derivative are predominant strigolactones in Arabidopsis. Plant Direct 4(5): 1–14
- Yoneyama K, Arakawa R, Ishimoto K, Kim HI, Kisugi T, Xie X, Nomura T, Kanampiu F, Yokota T, Ezawa T, et al. (2015) Difference in Striga-susceptibility is reflected in strigolactone secretion profile, but not in compatibility and host preference in arbuscular mycorrhizal symbiosis in two maize cultivars. New Phytol 206(3): 983–989
- Yoneyama K, Mori N, Sato T, Yoda A, Xie X, Okamoto M, Iwanaga M, Ohnishi T, Nishiwaki H, Asami T, et al. (2018) Conversion of carlactone to carlactonoic acid is a conserved function of MAX1 homologs in strigolactone biosynthesis. New Phytol 218(4): 1522–1533
- Zhang J, Mazur E, Balla J, Gallei M, Kalousek P, Medvedová Z, Li Y, Wang Y, Prát T, Vasileva M, et al. (2020) Strigolactones inhibit auxin feedback on PIN-dependent auxin transport canalization. Nat Commun 11: 3508
- Zhou W, Wang L, Zheng W, Yao W (2019) MaizeSNPDB: a comprehensive database for efficient retrieve and analysis of SNPs among 1210 maize lines. Comput Struct Biotechnol J 17(Nov): 1377–1383
- Zhu Z, Tan L, Fu Y, Liu F, Cai H, Xie D, Wu F, Wu J, Matsumoto T, Sun C (2013) Genetic control of inflorescence architecture during rice domestication. Nat Commun 4(1): 2200